

## Journal Pre-proofs

Jurassic picritic and potassic mafic dyke swarms in eastern China: Evidence for thermal erosion of the lithospheric mantle during Paleo-Pacific subduction

Wenjia Wang, Shuguang Song, Chao Wang, Mark B. Allen, Lifei Zhang, Xiaowei Li, Li Su

PII: S1342-937X(25)00043-7  
DOI: <https://doi.org/10.1016/j.gr.2025.02.012>  
Reference: GR 3433

To appear in: *Gondwana Research*

Received Date: 13 June 2024  
Revised Date: 18 January 2025  
Accepted Date: 24 February 2025



Please cite this article as: W. Wang, S. Song, C. Wang, M.B. Allen, L. Zhang, X. Li, L. Su, Jurassic picritic and potassic mafic dyke swarms in eastern China: Evidence for thermal erosion of the lithospheric mantle during Paleo-Pacific subduction, *Gondwana Research* (2025), doi: <https://doi.org/10.1016/j.gr.2025.02.012>

This is a PDF file of an article that has undergone enhancements after acceptance, such as the addition of a cover page and metadata, and formatting for readability, but it is not yet the definitive version of record. This version will undergo additional copyediting, typesetting and review before it is published in its final form, but we are providing this version to give early visibility of the article. Please note that, during the production process, errors may be discovered which could affect the content, and all legal disclaimers that apply to the journal pertain.

© 2025 Published by Elsevier B.V. on behalf of International Association for Gondwana Research.

# **Jurassic picritic and potassic mafic dyke swarms in Eastern China: evidence for thermal erosion of the lithospheric mantle during Paleo- Pacific subduction**

Wenjia Wang<sup>1, 2, 3</sup>, Shuguang Song<sup>†1</sup>, Chao Wang<sup>4</sup>, Mark B. Allen<sup>5</sup>, Lifei Zhang<sup>1, 2</sup>, Xiaowei Li<sup>2</sup>, Li Su<sup>6</sup>

<sup>1</sup> MOE Key Laboratory of Orogenic Belts and Crustal Evolution, School of Earth and Space Sciences, Peking University, Beijing 100871, China

<sup>2</sup> School of Earth Sciences and Resources, China University of Geosciences, Beijing 100083, China

<sup>3</sup> Key Laboratory of Mineral Resources in Western China (Gansu Province), School of Earth Sciences, Lanzhou University, Lanzhou 730000, China

<sup>4</sup> Department of Earth Sciences, The University of Hong Kong, Pokfulam Road, Hong Kong, China

<sup>5</sup> Department of Earth Sciences, University of Durham, Durham DH1 3LE, UK

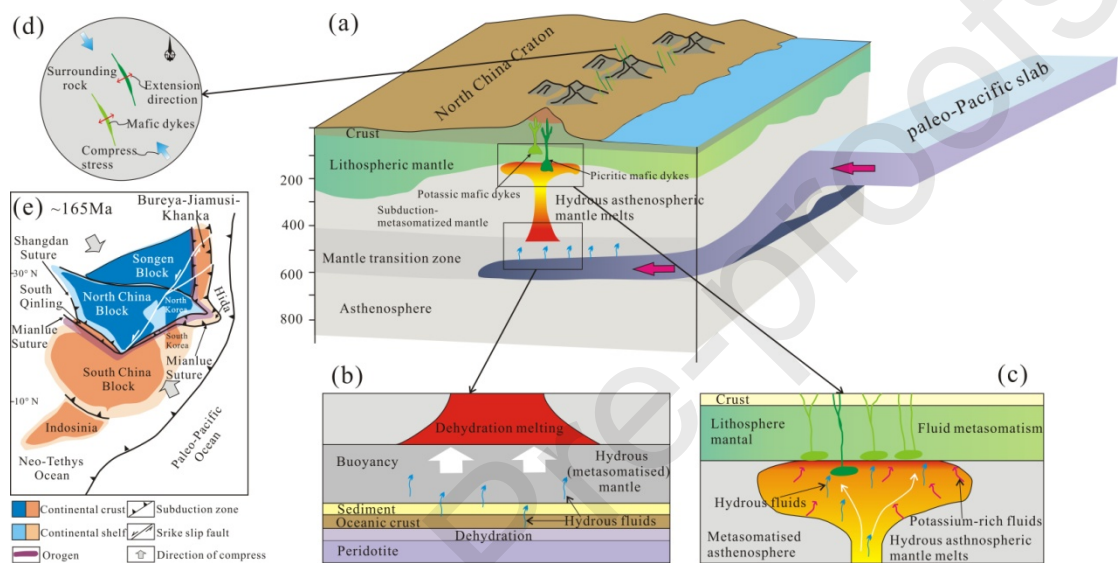
<sup>6</sup> Institute of Earth Sciences, State Key Laboratory of Geological Processes and Mineral Resources, China University of Geosciences, Beijing 100083, China

†Corresponding author: Shuguang Song (sgsong@pku.edu.cn)

## **Highlights**

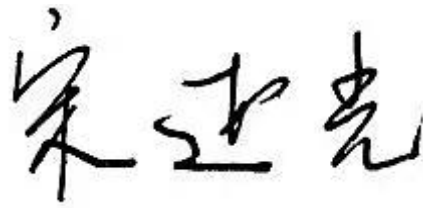
- Jurassic mafic dyke swarms indicate hydrous asthenospheric mantle melts rising from MTZ.
- The orientation of mafic dyke swarms indicates oblique Paleo-Pacific subduction in Jurassic.
- Thermal erosion would be the major factor for the lithospheric destruction during Jurassic.

## Graphical Abstract



## Declaration of Interest Statement

The authors declare that they have no known competing financial interests or personal relationships that could have appeared to influence the work reported in this paper.



Shuguang Song and co-authors

### CRediT authorship contribution statement

**Wenjia Wang:** Data curation, Formal analysis, Investigation, Writing – original draft. **Shuguang Song:** Conceptualization, Data curation, Formal analysis, Investigation, Writing – review & editing. **Chao Wang:** Investigation, Writing – review & editing. **Mark B. Allen:** Investigation, Writing – review & editing. **Lifei Zhang:** Data curation, Writing – review & editing. **Xiaowei Li:** Writing – review & editing. **Li Su:** Data curation, Investigation, Writing – review & editing.

### ABSTRACT

Paleo-Pacific subduction significantly impacted the structure and nature of the mantle in Eastern China. However, the thermal structure of the supra-subduction-zone mantle during the early stage of the Paleo-Pacific subduction has not been well constrained. Here, we present an integrated study involving field investigation, petrology, and geochemistry on two types of Jurassic (168-155 Ma) mafic dyke swarms in Western Liaoning, North China Craton (NCC), to trace the properties of the NCC mantle during the Jurassic. The picritic dyke swarms, trending NNW (330°–350°), show OIB-like geochemical signatures, with high mantle potential temperatures ( $T_p$ ) ranging from  $1498 \pm 52^\circ\text{C}$  to  $1535 \pm 56^\circ\text{C}$ . These picritic dyke swarms are derived from high-degree of partial melting of the asthenospheric mantle by a hot and hydrous asthenospheric melts rising from the mantle transition zone above the subducted slab. In contrast, the Jurassic potassic mafic dyke swarms, trending NNW (325°–345°), were formed by partial melting of the metasomatized lithospheric mantle during the

upwelling of the asthenospheric melts. We conclude that thermal erosion would be a major factor in the destruction of the lithospheric mantle beneath the NCC in the early stage of the Paleo-Pacific plate subduction.

**Keywords:** Jurassic picritic and potassic mafic dyke swarms, hydrous asthenospheric melts, Paleo-Pacific subduction, lithospheric destruction by thermal erosion, North China Craton

## 1. Introduction

Plate subduction is a complex geologic process occurring at convergent plate margins, where the subducting plate introduces crustal materials and volatiles into the mantle, triggering a series of significant physical and chemical processes (Stern, 2002; Zheng et al., 2016). Since the Jurassic, the subduction of the Paleo-Pacific Plate has had a profound impact on the mantle's structure and nature in eastern China. This subduction and subsequent rollback are widely recognized as the primary driving forces behind the thinning and destruction of the North China Craton (NCC) lithosphere (Wu et al., 2019; Ma and Xu, 2021). In contrast, lithospheric thinning is a geologic phenomenon frequently seen in the evolution of global cratons, such as the Indian Craton (Dessai et al., 2004), the North Atlantic Craton (Tappe et al., 2007, 2017), the Siberian Craton (Reichow et al., 2009), and the Brazilian Craton (Read et al., 2004). Lithospheric thinning involves the replacement of a thick, cold, and depleted continental lithospheric mantle with a thinner, hotter, and more compositionally fertile mantle (Gao et al., 2002). Furthermore, two prominent indicators of lithospheric thinning are the emergence of magma derived from the asthenosphere and the transition of magma sources from the lithospheric mantle to the asthenospheric mantle (Xu et al., 2009; Ma et al., 2014). Previous authors have proposed two main mechanisms for lithospheric thinning in the NCC: thermal-chemical erosion (Xu, 2001; Deng et al., 2004; Zheng et al., 2005) and rapid lithospheric delamination (Gao et al., 2004; Wu et al., 2005; Ma et al., 2014; Zhu et al., 2019; Chen et al., 2023). It is generally believed that significant thinning of the NCC lithosphere occurred during the Early Cretaceous (Ma et al., 2014; Dai et al., 2016; Zheng et al., 2018). However, the emergence of Jurassic magma derived from the asthenosphere in the NCC suggests that the nature of the mantle and the processes of lithospheric thinning in the early subduction zone of the Paleo-Pacific Plate are not yet well understood.

Water, along with other volatile components, may be transported by subducting plates into the mantle transition zone (MTZ) or even deeper into the mantle, undergoing a long and complex migratory and evolutionary process (Karato, 2011; Zheng et al., 2016). Geophysical observation and geodynamic modeling suggest that the hydrous mantle plume, also known as upwelling hydrous asthenospheric melts, can be generated by slab subduction into the MTZ at depths between 410-660 km (Katz et al., 2003; Karato, 2011; Kuritani et al., 2011; Wang et al., 2015; Blatter et al., 2022). The volcanic rocks associated with these hydrous asthenospheric melts represent significant magmatic activity originating from deep and hot mantle regions below the subduction zone (Shimizu et al., 2001; Liu et al., 2017; Blatter et al., 2022). Changbaishan in northeast China is one of the most typical hydrous mantle plume volcanoes that may have originated from the MTZ, as shown by geophysical studies (Kuritani et al., 2019). Furthermore, the upwelling of hydrous asthenospheric melts to the bottom of the continental lithosphere exposes this lithosphere to an anomalously hot thermal source, and raises the temperature above the solidus. The result is partial melting, thermal erosion, and eventual destruction of the lithosphere (Zhu et al., 2009; Richard and Iwamori, 2010; Grove et al., 2012).

Mafic/ultramafic dyke swarms, as mantle-derived magmas directly transferred through conduits to the crust, play important roles in tracing both the properties of the mantle source and the tectonic setting (Ernst et al., 1995). The low viscosity and fast migration velocity of the primary magmas makes mafic dyke swarms less prone to contamination during emplacement, offering a more direct reflection of the mantle source compositional features. Furthermore, the orientations of mafic dyke swarms can reveal the regional stress field (Gudmundsson, 2002). In this paper, we focus on two types of Jurassic mafic dyke swarms in the eastern NCC, i.e., OIB-like picritic dyke swarms and potassic dyke swarms, in the Western Liaoning region of the NCC. We suggest that hydrous asthenospheric melts might have been present beneath the NCC during the early stage of the Paleo-Pacific plate subduction, with thermal erosion likely playing a critical role in triggering the destruction of the craton.

## 2. Geological background

The NCC, is the largest and oldest cratonic block in China. It is composed mainly of Archean tonalitic-trondhjemitic-granodioritic (TTG) gneisses and high-grade metamorphic rocks with ages ranging between 3.8-2.5 Ga (Liu et al., 1992; Zhao et al., 2001; Kusky, 2011; Wang et al., 2019; Zhai et al., 2021; Wu et al., 2022). The craton mainly stabilized in the late Paleoproterozoic (Zhao et al., 2005). However, the eastern part of the NCC was strongly remobilized with intense deformation, and widespread magmatism and mineralization in the Mesozoic (Xu, 2001; Wu et al., 2005; Ma and Xu, 2021). In the Early Mesozoic, the final closure of the paleo-Asian Ocean and collision between the South and North China cratons resulted in major post-orogenic magmatism in the Triassic, which caused the first stage of lithospheric mantle destruction of the NCC (Yang et al., 2005; Yang et al., 2008b; Wang et al., 2021). With the subduction of the Jurassic Paleo-Pacific plate, the structure and composition of the mantle beneath the NCC were significantly impacted, resulting in the complete destruction of the NCC (Zhu et al., 2012; Zhang et al., 2014; Dong et al., 2019; Zhu and Xu, 2019; Fang et al., 2021; Chen et al., 2023). Concurrently, two giant igneous sub-provinces have been identified within the NCC during the Jurassic (175-155 Ma) and the Early Cretaceous (135-115 Ma) (Wu et al., 2019). These findings align with the magmatic peaks observed along the Taihang to Western Liaoning regions (Fig. 1a; Table S1).

Our study area is located in the Western Liaoning region of the eastern NCC, west of the Tanlu Fault (Fig. 1a). It is dominantly composed of Archean TTG basement with Middle Proterozoic to Paleozoic strata and well-developed Mesozoic igneous rocks (Fig. 1b; Peng and Guo, 2019; Wang et al., 2022). The granitic intrusions have been divided into three major suites: the Jiumen monzodiorites and monzogranites (190-182 Ma), the Xiaoyingzi granites (186-164 Ma), and the Houshihushan alkali granites (120-118 Ma) (Wu et al., 2006b; Yang et al., 2008a). Mafic and felsic dyke swarms intruded into the Mesozoic granitoid and Archean basement rocks, with variable lengths, widths, and orientations. Most of them are poorly studied except for lamprophyres (162-139 Ma) in the Taili area (Wan et al., 2019).

### 3. Field occurrence and petrography

The studied samples were collected from two regions in Western Liaoning, Eastern NCC (Fig. 1c). Each sample was selected from the center of the dykes in order to avoid possible crustal contamination.

In the Xingcheng region, a large number of mafic dyke swarms intrude into the Archean gneisses and the Jurassic plutons (Fig. 1d; Wu et al., 2006a). They are 0.5-20 m in width and have chilled margins with a consistent strike of mainly NNW ( $330^{\circ}$ - $340^{\circ}$ ; Fig. 1d1). In the Taili region, mafic dyke swarms intrude into the Neoproterozoic Suizhong granitic gneiss (Wang et al., 2016) and the Late Triassic porphyritic granite (Fig. 1e; Liang et al., 2015), with sharp, chilled margins. They show mainly NNW strikes ( $325^{\circ}$ - $350^{\circ}$ ; Fig. 1e1), with widths of 1-10 m.

The mafic dykes have fine-grained ophitic and porphyritic textures at the two margins (Figs. 2e, f) and the coarse-grained texture in the center of dykes (Figs. 2g, h). They can be divided into two groups based on their compositions. The first group is NNW-trending ( $330^{\circ}$ - $350^{\circ}$ ) picritic mafic dyke swarms (Figs. 2a, b). The mineral assemblage is amphibole (40-50 vol%), clinopyroxene (10-20 vol%), plagioclase (10-15 vol%), spinel (5 vol%), and accessory minerals. Olivine pseudocrystals altered by iddingsite can be observed in some samples (Fig. 2e). Cr-rich spinel occurs as fine-grained euhedral crystals within the groundmass or phenocrysts (Figs. 2e, g). The second group is green-coloured potassic mafic dyke swarms. They show the same NNW-trend ( $325^{\circ}$ - $345^{\circ}$ ) (Figs. 2c, d) and ophitic and porphyritic texture especially at the dyke margins, whereas the central regions displayed coarser grain sizes, where the ophitic texture was not that evident. Some samples have euhedral to subhedral clinopyroxene and amphibole phenocrysts. Their groundmass consists of clinopyroxene (15-25 vol%), amphibole (40-45 vol%), plagioclase (20-30 vol%), biotite (~2 vol%) and magnetite (Figs. 2g, h), with no spinel.

### 4. Analytical methods and results

The U-Pb dating analysis of zircon were conducted by LA-ICP-MS at the Wuhan SampleSolution Analytical Technology Co., Ltd., Wuhan, China. Major element compositions of minerals were determined using a JEOL JXA-8230 Electron Probe Microanalyzer (EPMA) at the Key Laboratory of Orogeny and Crustal Evolution, Ministry of Education, Peking University. Trace element analysis of minerals were conducted by LA-ICP-MS at the Center for High Pressure Science & Technology Advanced Research, Beijing, China. Additionally, whole-rock major and trace element compositions were analyzed in the Geological Lab Center, China University of Geosciences, Beijing (CUGB). Meanwhile, whole-rock Rb-Sr and Sm-Nd isotope compositions were determined at the Isotope Laboratory of the Tianjin Institute of Geology and Mineral Resources. Analytical methods involved in data acquisition, including sample preparation, instrument types, and their working conditions, reference materials, analytical accuracy, and precision, and data reduction schemes are

documented in the Supplementary Material.

#### 4.1 Zircon U-Pb geochronology

Four representative mafic dyke samples were selected for LA-ICP-MS zircon U-Pb dating, including the Taili picritic mafic dyke sample JX125-1 (Fig. 3a), Taili potassic mafic dyke samples JX124-1 and JX124-2 (Figs. 3b, c), Xingcheng picritic mafic dyke samples 12T3 (Fig. 3d). Ca. 50 zircon grains were separated from each sample, and LA-ICP-MS analyses are presented in Table S2. The cathodoluminescence (CL) images of representative zircons from these rocks are shown in Fig. 3.

Zircons from the dated samples are mostly euhedral-subhedral or irregular in shape, 20-200  $\mu\text{m}$  in size, with length to width ratios of 1:1 to 5:1. Some of these zircon grains show clear oscillatory zoning in CL images, indicative of a magmatic origin. Some grains are dark and have relatively blurry oscillatory zoning, consistent with a xenocrystic origin. A total of 15 spots were analyzed in 14 representative zircons from sample JX125-1. Ten of the analyzed zircons are xenocrysts with Paleoproterozoic  $^{207}\text{Pb}/^{206}\text{Pb}$  ages ranging from  $2424 \pm 28$  to  $2224 \pm 17$  Ma. Five zircon grains yield concordant  $^{206}\text{Pb}/^{238}\text{U}$  ages with a weighted mean of  $156 \pm 1.3$  Ma (MSWD = 0.39) (Fig. 3a), which is considered to represent the emplacement age of the picritic mafic dykes. A total of 18 spots were analyzed in 18 representative zircons from sample JX124-1. Six spots yield  $^{206}\text{Pb}/^{238}\text{U}$  ages between  $319 \pm 7$  Ma and  $255 \pm 4$  Ma, and these zircons are considered to have been captured during the ascent of mafic magmas. Six of the zircons from sample JX124-1 yield  $^{207}\text{Pb}/^{206}\text{U}$  ages of ca.  $2619 \pm 28$  to  $2062 \pm 25$  Ma, and are xenocrysts captured from the basement. Four zircon grains yield concordant  $^{206}\text{Pb}/^{238}\text{U}$  ages with a weighted mean of  $155 \pm 1.4$  Ma (MSWD = 0.02) (Fig. 3b), which is considered as the emplacement age of the potassic mafic dykes. For sample JX124-2, rejecting one spot with older  $^{206}\text{Pb}/^{238}\text{U}$  ages (194 Ma), the remaining 12 analyses yield a weighted mean  $^{206}\text{Pb}/^{238}\text{U}$  age of  $162 \pm 1.3$  Ma (MSWD = 0.68) (Fig. 3c), considered to represent the emplacement age of the potassic mafic dykes. A total of 15 spots were analyzed on 15 representative zircons from sample 12T3. Eight of the zircons are xenocrysts with Paleoproterozoic  $^{207}\text{Pb}/^{206}\text{Pb}$  ages ranging from  $2452 \pm 36$  to  $2217 \pm 33$  Ma. Six zircon grains yield concordant  $^{206}\text{Pb}/^{238}\text{U}$  ages with a weighted mean of  $168 \pm 1.3$  Ma (MSWD = 0.019) (Fig. 3d), which is considered to represent the emplacement age of the picritic mafic dykes.

#### 4.2 Mineral chemistry

##### 4.2.1 Minerals in picritic mafic dykes

Clinopyroxenes in picritic mafic dyke samples (JX123-1, JX125-1, and JX126-1) are mainly augite with Wo 27.11%-28.98%, En 43.45%-58.88%, and Fs 12.21%-27.53% (Fig. 4a; Table S3). Plagioclase in a few picritic samples has been altered into albite by zoisitization. Magmatic hornblende crystals in the picritic sample show consistent compositions, with  $\text{Ca}_B=1.78\text{-}2.03$ ,  $(\text{Na}+\text{K})_A=0.72\text{-}0.90$ ,  $\text{Ti}=0.09\text{-}0.48$ ,  $\text{Si}=5.87\text{-}6.51$ ,  $^{\text{VI}}\text{Al}<\text{Fe}^{3+}$ , and  $X_{\text{Mg}}$  between 0.69 and 0.85, classifying it as magensiohastingsite (Fig.

4b). Hornblendes in the picritic dykes have very low contents of Cr (aver. 183 ppm) and Ni (aver. 194 ppm) (Table S4). They show chandelier chondrite-normalized REE patterns, with a significant depletion of LREEs (Fig. S1a).

Chromian spinel is a ubiquitous accessory phase in Cr-rich igneous rocks and can be used to calculate the degree of partial melting of the mantle source, as well as distinguish between different tectonic settings, viz island arc, mantle-plume and mid-ocean ridge, and the partial melting degree of the mantle (Kamenetsky et al., 2001). Most spinels in picritic mafic dyke samples (JX123-1, JX125-1, and JX126-1) have high  $\text{TiO}_2$  (0.66-1.64 wt%), plotting within the field of ocean island basalts (OIB) (Fig. 4c), and  $\text{Cr}\# [100 \times \text{Cr} / (\text{Cr} + \text{Al}) = 61-74]$  values similar to those of Hawaiian picrites (Norman and Garcia, 1999).

#### **4.2.2 Minerals in potassic mafic dykes**

Clinopyroxene crystals in the potassic samples (JX124-1 and XC41) are homogeneous without zonation and mainly diopside in composition with  $\text{Wo}$  40.85%-47.86%,  $\text{En}$  37.83%-45.14%,  $\text{Fs}$  9.95%-13.71%, different from clinopyroxene in the picritic dykes (Fig. 4a). Plagioclases from the potassic sample are oligoclase (Table S3). Most magmatic hornblende crystals show consistent compositions of magensiohastingsite (Fig. 4b). They have low contents of Cr (aver. 101 ppm) and Ni (aver. 73 ppm) (Table S4), and display parallel and convex-upward REE patterns (Fig. S1b).

### **4.3 Whole-rock major and trace elements**

Thirty-five representative samples of mafic dykes from the two studied regions were selected for whole-rock major and trace element analyses, and the results are shown in Table S5. Major element contents were normalized to 100% on a volatile-free basis in all diagrams. According to their geochronology and geochemical features, the mafic dyke swarms can be divided into two groups, including the Jurassic picritic mafic dyke swarms, and Jurassic potassic mafic dyke swarms (Fig. 5).

#### **4.3.1 Picritic mafic dyke swarms**

Jurassic picritic mafic dyke swarms are characterized by high contents of  $\text{MgO}$  (10.28-18.55 wt%),  $\text{Mg}\#$  (66-75), Cr (574-1438 ppm), and Ni (208-500 ppm), and low contents of  $\text{Al}_2\text{O}_3$  (8.27-13.14 wt%) mainly plotting in the fields of picrite and basalt in the TAS and  $\text{SiO}_2$ - $\text{MgO}$  diagram (Figs. 5a,b) and in the alkaline-basalt field in the Nb/Y versus Zr/Ti diagram (Fig. 5c), with medium to high  $\text{K}_2\text{O}$  contents (0.56-1.73 wt%) (Fig. 5d). They show significant enrichment of light rare-earth elements (LREE) with high  $(\text{La}/\text{Yb})_{\text{N}} = 16-25$  in the chondrite-normalized REE diagram (Fig. 6a), and OIB-affinity with enrichment of Nb and Ta in the primitive mantle-normalized diagram (Fig. 6b).

#### **4.3.2 Potassic mafic dyke swarms**

The Jurassic potassic mafic dyke swarms have SiO<sub>2</sub> content of 49.47-58.46 wt%, total alkalis (Na<sub>2</sub>O+K<sub>2</sub>O) contents of 5.17-8.66 wt%, and mainly plot in the fields from trachybasalt to trachyandesite (Fig. 5a). In the Nb/Y versus Zr/Ti classification diagram, most of them plot in the field of alkaline-basalt (Fig. 5c). They have high K<sub>2</sub>O contents (1.81-4.98 wt%) and thus belong to high-K to shoshonitic series (Fig. 5d). They have relatively low MgO (3.09-8.54 wt%) and Mg# (44-59), Cr (11-338 ppm), and Ni (2-150 ppm), and high Al<sub>2</sub>O<sub>3</sub> (13.30-17.66 wt%) and P<sub>2</sub>O<sub>5</sub> (0.49-1.05 wt%). They also display enrichment in LREE ((La/Yb)<sub>N</sub> =18-32) (Fig. 6c), but strong depletion in HFSEs (Nb, Ta, and Ti) (Fig. 6d), incomparable to the picritic OIB-like dykes.

#### 4.4 Whole-rock Sr-Nd isotopes

The Jurassic picritic mafic dyke swarms have narrow ranges of (<sup>87</sup>Sr/<sup>86</sup>Sr)<sub>i</sub> ratios (0.704488-0.704858) and εNd(t) values (-2.2 to 0.9) (Table S6), extending along the mantle array, suggesting that they could be derived from an asthenospheric mantle. The Jurassic potassic mafic dyke swarms have relatively higher (<sup>87</sup>Sr/<sup>86</sup>Sr)<sub>i</sub> ratios (0.706826-0.707239) and strongly negative εNd(t) values (-15.7 to -15.2) (Table S6), with single-stage model ages ranging from 1837 to 1963 Ma (Fig. 7).

### 5. Discussion

#### 5.1 Evaluation of elemental mobility and crustal contamination

Before discussing the petrogenesis of the Jurassic mafic dyke swarms, it is important to evaluate the potential effects of low-temperature alteration after magma emplacement. Although the mafic dyke swarms display high loss-on-ignition (LOI) values, 2.37-8.25 wt% for the potassic mafic dykes and 1.12-4.64 wt% for the picritic mafic dyke swarms (Table S5), nevertheless, correlations between some trace elements (La, Th, Ce, Nd, etc.; see Fig. S2) and Zr show consistent trace element characteristics of primitive igneous rocks (Fig. 6). Therefore, these elements can be used to decipher their petrogenesis. In contrast, some elements (e.g., Na, Rb, Sr) were likely modified by alteration and metamorphism, so these mobile elements were avoided in petrogenetic interpretation.

Crustal contamination is a prevalent phenomenon in the process of magma evolution, which can potentially alter the trace element and isotopic composition of the host magma. These mafic dykes could have potentially assimilated crustal materials during their emplacement, as supported by the presence of ancient zircon xenocrysts. However, the potassic mafic dyke swarms have much higher Rb, Sr, and Ba contents than the NCC crust (Rb = 59-68 ppm; Sr = 350-336 ppm; Ba = 677-688 ppm; Gao et al., 1998). In addition, their (<sup>87</sup>Sr/<sup>86</sup>Sr)<sub>i</sub> ratios and εNd(t) values do not vary linearly with SiO<sub>2</sub> and MgO (see Fig. S3), indicating that they also did not experience significant crustal assimilation. On the other hand, two picritic mafic dyke samples have negative εNd(t) values (~ -2.3) (Fig. S4), suggesting a limited degree of crustal contamination. The picritic mafic dykes are also characterized by low SiO<sub>2</sub>, high MgO, Cr, and Ni, positive Nb, Ta, high εNd(t) values, and low(<sup>87</sup>Sr/<sup>86</sup>Sr)<sub>i</sub> ratios (Figs. 5, 6, 7; Table S5), which

imply a depleted mantle origin and argue against significant crustal contamination. In addition, they show no change in  $\text{TiO}_2$  and  $\text{P}_2\text{O}_5$  content with decreasing MgO values (except for sample 12C-1) (Figs. S4a, b), which is inconsistent with significant crustal contamination that normally decreases the  $\text{TiO}_2$  and  $\text{P}_2\text{O}_5$  contents (Zhao and Zhou, 2007). Moreover, the picritic mafic dyke swarms show uniform trace element patterns with weak negative Zr and Hf anomalies relative to the primitive mantle (Fig. 6b), which is inconsistent with extensive crustal contamination (e.g., Zhao and Zhou, 2007). Additional support for this conclusion is provided by the absence of a positive correlation between  $(^{87}\text{Sr}/^{86}\text{Sr})_i$  ratios and  $\text{SiO}_2$  and MgO contents in the whole-rock (Wang et al., 2021) (Fig. S3). Thus, the impact of crustal contamination on the magma evolution of both potassic and picritic mafic dyke swarms is likely to be limited.

## 5.2 Tracing the origin of the hydrous asthenospheric mantle by Jurassic picritic mafic dyke swarms

### 5.2.1 Geochemical evidence for an asthenospheric mantle origin

Lines of evidence reveal that both picritic mafic dyke swarms and potassic dyke swarms are primitive melts, rather than formed by amphibole accumulation. (1) Most dykes show ophitic and porphyritic textures at the margins and the coarse-grained texture at the center, rather than the accumulated texture, and they have uniform compositions from the margin to the center of dykes. (2) The REE patterns of amphiboles are different from those of their host whole-rocks, especially the LREE (Fig. S1). (3) Amphiboles can easily fractionate MREE and HREE elements because Dy is more compatible with amphibole than Yb. Thus, during magmatic differentiation, the formation of amphibole cumulates produces an amphibole signal, which means that Dy/Yb decreases with the increase of  $\text{SiO}_2$  (Davidson et al., 2007). However, the  $\text{SiO}_2$  vs. Dy/Yb plot of the picritic mafic dykes does not show a decreasing trend (Fig. S4c). (4) Picritic mafic dykes show a negative correlation between  $\text{SiO}_2$  and Mg# (Fig. S4d), which also rules out the origin by mineral accumulation (e.g., Dessimoz et al., 2012; Elemér et al., 2015; Xu et al., 2019).

Picrite and komatiite are representative rocks that originate from asthenospheric mantle, serving as useful indicators of high-temperature mantle sources (Su et al., 2021). Chromian spinels in the picritic mafic dyke samples exhibit low  $\text{Al}_2\text{O}_3$  and high Cr#, similar to spinels found in Hawaii picrites and basaltic komatiites (Norman and Garcia, 1999), implying an asthenospheric source. In addition, the Jurassic picritic mafic dyke swarms possess typical OIB geochemical characteristics such as the positive Nb-Ta, and low  $(^{87}\text{Sr}/^{86}\text{Sr})_i$  and high  $\epsilon\text{Nd}(t)$  values, resembling Cenozoic Changbaishan basalts and Hawaiian picrites (Figs. 6, 7; Kuritani et al., 2009). As shown in Figs. 8a, c, d, all samples are plotted near the OIB field with no significant influence of subduction metasomatism, and their Nb/U (35-97) and Ce/Pb (6-36) ratios are comparable to those of MORB and OIB (Nb/U =  $47 \pm 10$ , Ce/Pb =  $25 \pm 5$ ; Hofmann et al. (1986)). All of the above features, as well as their Nb/La versus La/Yb systematics (Fig. 8b), suggest that the dyke swarms were derived from the asthenospheric mantle.

### 5.2.2 A hydrous asthenospheric mantle origin

Water, being a strongly incompatible element, tends to preferentially enter the melt phase during mantle melting. This incorporation alters the melt's structure and significantly impacts its equilibrium with the residual solid phase (Kelley and Cottrell, 2009). There is growing evidence that water plays a crucial role in processes ranging from low degrees of partial melting at the lithosphere-asthenosphere boundary to the high degrees of partial melting necessary for forming large igneous provinces (Xia et al., 2022). The formation of hydrous mantle plumes above the MTZ subducting plate at depths of 410-660 km is a typical example (Wang et al., 2015), and water serves as a plausible source of buoyancy for these plumes (Richard and Iwamori, 2010). It is believed that mantle plumes are caused by thermal buoyancy driven by steep thermal gradients at the core-mantle boundary, as evidenced by their high mantle potential temperature (Herzberg and Gazel, 2009). Primitive magmas from normal mantle plumes like Hawaii are typically dry and lack hydrous minerals. However, recent evidence suggests that some mantle plumes may not be significantly hotter than the ambient mantle, indicating that thermal buoyancy is not their primary cause (Kuritani et al., 2019). Furthermore, the basaltic oceanic crust (eclogite) and sediments of the Paleo-Pacific plate are also unlikely sources of buoyancy due to their higher density compared with the surrounding peridotite (Aoki and Takahashi, 2004). Conversely, hydrous mantle peridotite has a lower density than its dry counterpart, and the density of hydrous fluids and partial melts may also be lower than that of the host peridotite in the MTZ, leading to the dehydration and melting of water-rich asthenospheric mantle material. This process results in the formation of upwelling hydrous asthenospheric melts (Karato, 2011).

Water contents of mafic magmas can be estimated using the hygrometer of Perinelli et al. (2016), and the calculated method can be expressed as following Eqs. (1):

$$\text{wt\% H}_2\text{O} = a\text{DiHd} + b\text{EnFs} + c\text{CaTs} + d\text{Jd} + e\text{CaTi} + f\ln P + gT + k \quad (1)$$

where DiHd = diopside + hedenbergite, EnFs = enstatite + ferrosilite, CaTs = Ca-Tschemmak, Jd = jadeite, CaTi = CaTi-Tschemmak,  $a = 39.60$ ,  $b = 29.48$ ,  $c = 41.76$ ,  $d = 39.58$ ,  $e = 0.44$ ,  $f = 0.14$ ,  $g = -0.01$ ,  $k = -27.53$ ,  $P$  is in MPa, and  $T$  is in °C.

The studied Jurassic picritic mafic dyke samples in the eastern NCC contain large amounts of hornblende (40-50%), proving that their parent magmas are water-rich. Using the hygrometer of Perinelli et al. (2016), we estimate the H<sub>2</sub>O contents of the picritic samples to be between 0.6% and 1.8% in the melt (Table S3), similar to the water contents (1.2-1.8 wt.%) of the Changbaishan basalts (Kuritani et al., 2019).

### 5.2.3 Melting degree and P-T conditions

Jurassic picritic mafic dyke samples, with high Mg# (=66-75), are enriched in compatible elements (Cr, Co, and Ni) (Table S5), which suggest a high-degree melting of the mantle source. To estimate the relationship between Cr# and the degree of

melting ( $F$ ), we use the formula  $F = 10 \ln (\text{Cr} \#) + 24$  given by Hellebrand et al. (2001) and obtain a melting degree of 19.0%-21.0% for the picritic mafic dykes (Table S3). The results are identical to the picrites in the Baoshan-Gongshan Block of the northern Sibumasu terrane, southwest China (Su et al., 2021), but higher than most N-MORB.

Using a Si activity thermobarometer (Lee et al., 2009), we calculate the melting conditions for primary magmas of picritic mafic dyke samples and the results are listed in Table S7 and illustrated in Figure 9. The mean values of  $T_p$  are  $1535 \pm 56^\circ\text{C}$  and  $1498 \pm 52^\circ\text{C}$  based on different water contents in the melt of 0.6 and 1.8 wt%, respectively, which are higher than the  $T_p$  of normal upper ambient mantle ( $1350^\circ\text{C}$ ; McKenzie and Bickle, 1988), but lower than the calculated  $T_p$  of the Hawaiian hotspot picrites ( $1630 \pm 90^\circ\text{C}$ ; Fig. 9). The melting pressures range from 2.4 to 4.7 GPa.

### 5.3 Melting of the enriched lithospheric mantle during plume upwelling

The Jurassic potassic mafic dyke samples exhibit high potassium contents and crust-like trace element signatures, characterized by enrichment of LREEs and LILEs and depletion of HFSEs. The Sr-Nd isotopes of the potassic mafic dykes differ significantly from the MORB-type or OIB-type asthenospheric mantle-derived rocks, and they are similar to contemporaneous mafic rocks in the NCC (Figs. 6c, d; Table S6), indicating that the potassic mafic dyke swarms were formed by partial melting of the enriched lithospheric mantle. Moreover, the Nb/La versus La/Yb ratios of these potassic mafic dyke samples fall within the range of magmas from the lithospheric mantle (Fig. 8b).

The presence of potassium-rich mineral phases in magmatic sources is essential for the formation of the potassic mafic dykes (Chu et al., 2013). Based on the previous discussion, it is believed that potassium-rich materials were formed in the lithospheric mantle by metasomatism of potassium-rich melts or fluids. Jurassic potassic mafic dykes show variable Sr/Th and Th/Ce ratios with constant Ba/Th and Th/Nd values (Fig. S5), suggesting that the lithospheric mantle was metasomatized by potassium-rich fluids (Elburg and Foden, 1999). However, the origin of potassium-rich fluids is subject to various interpretations, with proposals including delaminated SCLM (Choi et al., 2006), deep asthenospheric mantle (Tappe et al., 2023), delaminated lower continental crust (Chu et al., 2013) or mantle transition zone (Murphy et al., 2002). Based on the average Nb/U ratio (22; Table S5) of the Jurassic potassic mafic dykes, which is notably lower than that of MORBs and OIBs ( $\text{Nb}/\text{U} = 47 \pm 10$ ; Hofmann et al. (1986)), and lower crust ( $\text{Nb}/\text{U} = 25$ ; Gao et al. (1998)), as well as their Sr-Nd isotopes being different from an ancient sub-continental lithospheric mantle, it appears that the enriched lithospheric mantle source may not be associated with lower crustal delamination. We utilize a Si activity thermobarometer (Lee et al., 2009) to determine the  $T_p$  of potassic mafic dyke samples. The mean  $T_p$  values were  $1156 \pm 37^\circ\text{C}$  and  $1140 \pm 32^\circ\text{C}$  for water contents of 1.5 wt% and 3.3 wt% (Table S3), respectively. These values are consistent with those expected for the lithospheric mantle ( $1180^\circ\text{C}$ ; Sun et al., 2014) but lower than those of the mantle transition zone ( $1250^\circ\text{C}$ , Kuritani et al., 2011). The variations of La/Ba versus La/Nb ratios (Fig. 8a),  $(\text{Hf}/\text{Sm})_N$  versus  $(\text{Ta}/\text{La})_N$  ratios (Fig. 8c), and Th/Yb

versus Nb/Yb ratios (Fig. 8d) suggest a lithospheric mantle source modified by subduction. Therefore, the potassium-rich fluids that contributed to the Jurassic potassic mafic dykes most likely originated from the Paleo-Pacific subduction zone.

Additionally, Duggen et al. (2005) proposed a K/Yb vs. Dy/Yb plot to determine the mantle source composition and the partial melting degree of the parent magma. The Dy/Yb values of the potassic mafic dykes range from 2.06 to 2.57 (average value 2.40), indicating partial melting in the spinel-garnet transition zone (Fig. 10). The wide range of their K/Yb values (9.84-24.06) may reflect different partial melting degrees (Liu et al., 2020). Overall, the potassic mafic dyke swarms were formed by the partial melting of a bearing lherzolite lithospheric mantle in the spinel-garnet transition zone. We propose that partial melting of the metasomatized lithospheric mantle was induced by the upwelling hydrous asthenospheric mantle melts.

#### **5.4 Thermal erosion triggered the lithosphere destruction beneath the NCC**

Numerous studies have demonstrated significant lithospheric thinning occurred in the NCC, with its thickness decreasing from 200 km in the Paleozoic to 80-100 km in the Cenozoic (Gao et al., 2002). Meanwhile, the subduction of the Paleo-Pacific plate was a key factor influencing the thinning of the eastern NCC from the Jurassic to the Cretaceous, independent of the tectonic systems of the Paleo-Asian and Mongolian-Okhotsk Oceans (Zhu and Xu, 2019). The westward subduction of the Paleo-Pacific plate led to a large number of late Mesozoic igneous rocks in the eastern NCC (Zhang et al., 2014; Wu et al., 2019). Moreover, multiple lines of evidence suggest that the destruction of the NCC had already begun by the Late Jurassic (Jiang et al., 2010; Deng et al., 2017). However, the earliest reported asthenospheric mantle-sourced magmas are the Early Cretaceous (121 Ma) lamprophyres in the Jiaodong Peninsula, which exhibit trace element compositions and depleted isotopic compositions similar to OIB (Ma et al., 2014). Therefore, our findings of Jurassic picritic and potassic mafic dyke swarms provide direct evidence of Jurassic lithosphere thinning in the NCC, implying that subduction of the Paleo-Pacific plate beneath the NCC may have initiated in the Middle Jurassic (168 Ma), which plausibly explains the emergence of the giant igneous sub-provinces in the NCC during the Jurassic (Fig. 1a; Table S1).

It is shown that the NCC underwent a tectonic transition from compression to extension during the Cretaceous, influenced by the rollback of the Paleo-Pacific plate (Wu et al., 2019; Ma and Xu, 2021). Therefore, we can conclude that the Jurassic asthenospheric mantle source samples in this study were not formed by rapid lithospheric delamination, but as a result of thermal erosion. Strong variations in lithosphere thickness and thermal structure at the Craton margin may have caused transient small-scale mantle convection (Tappe et al., 2016). During the Jurassic, the subducting Paleo-Pacific plate beneath the NCC became dehydrated and partially melted. The melts/fluids released from the Paleo-Pacific plate altered the overlying lithospheric mantle (Zheng et al., 2018). We propose that hydrous asthenospheric mantle melts, inferred from the studied picritic mafic dyke swarms, formed by the

subducted slab in the MTZ, rose from the upper mantle to the bottom of the lithosphere. The high temperature and high water content of these melts effectively weakened the bottom of the lithosphere and mixed the lower part of the lithosphere into the asthenospheric mantle, leading to the lithospheric thinning in the NCC (Figs 11a, b, c).

The Jurassic transformation of the tectonic regime in Eastern China played a crucial role in the destruction and thinning of the NCC and also provided valuable insights into the Paleo-Pacific plate subduction. Dyke swarms can be used to reconstruct paleo-stress fields (Ray et al., 2007). The orientation of a subparallel dyke swarm can reflect the direction of maximum horizontal compressive stress at the time of their emplacement in the region (Gudmundsson, 2002). The mafic dyke swarms sampled in this study are reliable paleo-stress indicators because they were not significantly metamorphosed or deformed. The orientation of the Jurassic picritic and potassic mafic dykes, which strike NNW-SSE ( $325^{\circ}$ - $350^{\circ}$ ) and dip at angles of  $80^{\circ}$ - $90^{\circ}$ , clearly indicates WSW-ENE extension in the Western Liaoning region of the NCC (Fig 11d).

The Early Jurassic Paleo-Pacific plate began to subduct, continuously releasing potassium-rich fluids that contributed to the further metasomatism of the continental lithospheric mantle. By the Middle Jurassic, the Paleo-Pacific plate had subducted to the MTZ, with the hydrous mantle peridotite beneath the basaltic oceanic crust and/or the peridotite in the MTZ above the slab serving as the constituent buoyancy sources for hydrous asthenospheric mantle melts beneath the NCC. The thermal mantle melts lowered the solidus of the ancient lithospheric mantle as it crossed the upper mantle to the bottom of the lithosphere (Guo et al., 2020; Sun et al., 2020). Melt generation began when the mantle temperature intersected the solidus. This process promoted the gradual melting of the ancient lithospheric mantle, which effectively weakened and destabilized the bottom of the lithosphere, resulting in lithosphere thinning and the generation of large-scale magmatism (Niu, 2021). Therefore, we propose that thermal erosion, possibly accompanied by a hydrous mantle plume, would be a major factor in the destruction of the lithospheric mantle beneath the NCC in the early stage of the Paleo-Pacific plate subduction, as depicted in Figure 11e. Decompression melting of the upwelling asthenosphere produced OIB-type magmas, and thermally eroded metasomatized lithospheric mantle also melted. These magmas ascended along the ENE-WSW extensional zone to form Jurassic picritic and potassic mafic dyke swarms in the NCC.

## 6. Conclusions

(1) The Jurassic mafic dyke swarms (168-155Ma) in the Eastern NCC can be divided into two types, namely the picritic dyke swarms trending NNW-SSE ( $330^{\circ}$ - $350^{\circ}$ ) and the potassic dyke swarms also trending in an NNW-SSE ( $325^{\circ}$ - $345^{\circ}$ ) direction.

(2) The Paleo-Pacific plate subducted into the MTZ and provided buoyancy generated by water, thus forming hydrous asthenospheric mantle melts. The mantle potential temperature of the picritic mafic dyke swarms ranges from  $1498 \pm 52^{\circ}\text{C}$  to

1535 ± 56°C, with a melting degree of 19.0%-21.0%, and they were derived from high-degree melting of the asthenosphere mantle.

(3) Upwelling of the hot hydrous asthenospheric melts triggered partial melting of the metasomatized lithospheric mantle and formed the synchronous potassic mafic dyke swarms.

(4) The orientation of the Jurassic picritic and potassic mafic dyke swarms indicates a WSW-ENE extension in the NCC. Thermal erosion would be the major factor in the destruction of the lithospheric mantle beneath the NCC in the early stage of the Paleo-Pacific plate subduction.

### **CRedit authorship contribution statement**

**Wenjia Wang:** Data curation, Formal analysis, Investigation, Writing – original draft. **Shuguang Song:** Conceptualization, Data curation, Formal analysis, Investigation, Writing – review & editing. **Chao Wang:** Investigation, Writing – review & editing. **Mark B. Allen:** Investigation, Writing – review & editing. **Lifei Zhang:** Data curation, Writing – review & editing. **Xiaowei Li:** Writing – review & editing. **Li Su:** Data curation, Investigation, Writing – review & editing.

### **Acknowledgements**

This study was supported by the National Key Research and Development Program of China (2019YFA0708503) and China National Petroleum Corporation-Peking University Strategic Cooperation Project of Fundamental Research. Thanks to Yihu Zhang for his help during fieldwork, to Zhenyu Chen, Xiaoli Li, Meihui Wang, and Jintao Zhu for their help with electron microprobe analyses, to Renbiao Tao, Nan Li and Wenbo Xu for their help with trace element analyses of minerals, to Le Wan, Pu Sun and Pengyuan Guo for discussions. We would like to thank Editor-in-Chief Prof. M. Santosh, Associate Editor Prof. Sebastian Tappe and an anonymous reviewer for their thorough and constructive review comments, which significantly improved the quality of this manuscript.

### **Supplemental material**

The supplemental material includes: Figure S1 to S5, Tables S1 - S7.

### **References**

- Aoki, I., Takahashi, E., 2004. Density of MORB eclogite in the upper mantle. *Phys. Earth Planet. Inter.* 143-144, 129-143.  
<https://doi.org/10.1016/j.pepi.2003.10.007>.
- Blatter, D., Naif, S., Key, K., Ray, A., 2022. A plume origin for hydrous melt at the lithosphere–asthenosphere boundary. *Nature* 604 (7906), 491-494.  
<https://doi.org/10.1038/s41586-022-04483-w>.

- Chen, H., Tang, M., Song, S., 2023. Catastrophic craton destruction via wholesale lithosphere delamination. *Geology* 51 (5), 460-464. <https://doi.org/10.1130/G50803.1>.
- Choi, S. H., Mukasa, S. B., Kwon, S. T., Andronikov, A. V., 2006. Sr, Nd, Pb and Hf isotopic compositions of late Cenozoic alkali basalts in South Korea: Evidence for mixing between the two dominant asthenospheric mantle domains beneath East Asia. *Chem. Geol.* 232 (3), 134-151. <https://doi.org/10.1016/j.chemgeo.2006.02.014>.
- Chu, Z. Y., Harvey, J., Liu, C. Z., Guo, J.-H., Wu, F. Y., Tian, W., Zhang, Y. L., Yang, Y. H., 2013. Source of highly potassic basalts in northeast China: Evidence from Re–Os, Sr–Nd–Hf isotopes and PGE geochemistry. *Chem. Geol.* 357, 52-66. <https://doi.org/10.1016/j.chemgeo.2013.08.007>.
- Davidson J. Turner, H. Handley, C. MacPherson, A. Dosseto, 2007. Amphibole “sponge” in arc crust? *Geology* 35, 787-790. <https://doi.org/10.1130/G23637A.1>.
- Dai L. Q., Zheng Y. F., Zhao Z. F., 2016. Termination time of peak decratonization in North China: Geochemical evidence from mafic igneous rocks. *Lithos*, 240-243, 327-336. <https://doi.org/10.1016/j.lithos.2015.11.014>.
- Deng, J. F., Mo, X. X., Zhao, H. L., Wu, Z. X., Luo, Z. H., Su, S. G., 2004. A new model for the dynamic evolution of Chinese lithosphere: ‘continental roots–plume tectonics’. *Earth-Sci. Rev.* 65 (3), 223-275. <https://doi.org/10.1016/j.earscirev.2003.08.001>.
- Deng, J., Liu, X., Wang, Q., Dilek, Y., Liang, Y., 2017. Isotopic characterization and petrogenetic modeling of Early Cretaceous mafic dike–Lithospheric extension in the North China craton, eastern Asia. *GSA Bulletin*, 129 (11-12), 1379-1407. <https://doi.org/10.1130/B31609.1>.
- Dessai, A.G., Markwick, A., Vaselli, O., Downes, H., 2004. Granulite and pyroxenite xenoliths from the Deccan Trap: insight into the nature and composition of the lower lithosphere beneath cratonic India. *Lithos* 78, 263-290. <https://doi.org/10.1016/j.lithos.2004.04.038>.
- Dessimoz, M., Müntener, O., Ulmer, P. A., 2012. Case for hornblende dominated fractionation of arc magmas: the Chelan Complex (Washington Cascades). *Contrib. Mineral. Petrol.* 163, 567-589. <https://doi.org/10.1007/s00410-011-0685-5>.
- Dong, J., Song, S., Su, L., Li, Y., Yang, L., Wang, C., Xu, B., 2019. Onset of the North-South Gravity Lineament, NE China: Constraints of Late Jurassic bimodal volcanic rocks. *Lithos* 334-335, 58-68.

<https://doi.org/10.1016/j.lithos.2019.03.016>.

- Duggen, S., Hoernle, K., Van, D. B. P., Garbe.S. D., 2005. Post-Collisional Transition from Subduction- to Intraplate-type Magmatism in the Westernmost Mediterranean: Evidence for Continental-Edge Delamination of Subcontinental Lithosphere. *J. Petrol.* 6, 1155-1201. <https://doi.org/10.1093/petrology/egi013>.
- Elburg, M. A., Foden, J., 1999. Geochemical response to varying tectonic settings: an example from southern Sulawesi (Indonesia). *Geochim. Cosmochim. Acta* 63 (7), 1155-1172. [https://doi.org/10.1016/S0016-7037\(98\)00298-1](https://doi.org/10.1016/S0016-7037(98)00298-1).
- Ernst, R. E., Head, J. W., Parfitt, E., Grosfils, E., Wilson, L., 1995. Giant radiating dyke swarms on Earth and Venus. *Earth-Sci. Rev.* 39(1-2), 1-58. [https://doi.org/10.1016/0012-8252\(95\)00017-5](https://doi.org/10.1016/0012-8252(95)00017-5).
- Fang, W., Dai, L. Q., Zheng, Y. F., Zhao, Z. F., Ma, L. T., Zhao, K., 2021. Identification of Jurassic mafic arc magmatism in the eastern North China Craton: Geochemical evidence for westward subduction of the Paleo-Pacific slab. *GSA Bulletin* 133 (7-8), 1404-1420. <https://doi.org/10.1130/B35787.1>.
- Flèche, M. R. L., Camiré, G., Jenner, G. A., 1998. Geochemistry of post-Acadian, Carboniferous continental intraplate basalts from the Maritimes Basin, Magdalen Islands, Québec, Canada. *Chem. Geol.* 148 (3), 115-136. [https://doi.org/10.1016/S0009-2541\(98\)00002-3](https://doi.org/10.1016/S0009-2541(98)00002-3).
- Elemér Pál-Molnár, Anikó Batki, Enikő Almási, Balázs Kiss, Brian G.J. Upton, Gregor Markl, Nicholas Odling, 2015. Szabolcs Harangi, Origin of mafic and ultramafic cumulates from the Ditrău Alkaline Massif, Romania. *Lithos* 239, 1-18. <https://doi.org/10.1016/j.lithos.2015.09.022>.
- Gao, S., Luo, T. C., Zhang, B. R., Zhang, H. F., Han, Y. W., Zhao, Z. D., Hu, Y. K., 1998. Chemical composition of the continental crust as revealed by studies in East China. *Geochim. Cosmochim. Acta* 62 (11), 1959-1975. [https://doi.org/10.1016/S0016-7037\(98\)00121-5](https://doi.org/10.1016/S0016-7037(98)00121-5).
- Gao, S., Rudnick, R., Yuan, H., Liu, X., Liu, Y., Xu, W., Ling, W., Ayers, J., Wang, X., Wang, Q., 2004. Recycling lower continental crust in the North China craton. *Nature* 432 (7019), 892-897. <https://doi.org/10.1038/nature03162>.
- Gao, S., Rudnick, R. L., Carlson, R. W., McDonough, W. F., Liu, Y. S., 2002. Re-Os evidence for replacement of ancient mantle lithosphere beneath the North China craton. *Earth Planet. Sci. Lett.* 198 (3), 307-322. [https://doi.org/10.1016/S0012-821X\(02\)00489-2](https://doi.org/10.1016/S0012-821X(02)00489-2).
- Grove, T. L., Till, C. B., Krawczynski, M. J., 2012. The Role of H<sub>2</sub>O in Subduction Zone Magmatism. *Annu. Rev. Earth Planet. Sci.* 40 (1), 413-439. <https://doi.org/10.1146/annurev-earth-042711-105310>.

- Gudmundsson, A., 2002. Emplacement and arrest of sheets and dykes in central volcanoes. *J. Volcanol. Geotherm. Res.* 116 (3), 279-298. [https://doi.org/10.1016/S0377-0273\(02\)00226-3](https://doi.org/10.1016/S0377-0273(02)00226-3).
- Guo, P., Niu, Y., Sun, P., Gong, H., Wang, X., 2020. Lithosphere thickness controls continental basalt compositions: An illustration using Cenozoic basalts from eastern China. *Geology* 48 (2), 128-133. <https://doi.org/10.1130/G46710.1>.
- Hanyu, T., Kimura, J. I., Katakuse, M., Calvert, A. T., Sisson, T. W., Nakai, S. i., 2010. Source materials for inception stage Hawaiian magmas: Pb-He isotope variations for early Kilauea. *Geochem. Geophys. Geosyst.* 11 (3), Q0AC01. <https://doi.org/10.1029/2009GC002760>.
- Hellebrand, E., Snow, J. E., Dick, H. J. B., Hofmann, A. W., 2001. Coupled major and trace elements as indicators of the extent of melting in mid-ocean-ridge peridotites. *Nature* 410 (6829), 677-681. <https://doi.org/10.1038/35070546>.
- Herzberg, C., Gazel, E., 2009. Petrological evidence for secular cooling in mantle plumes. *Nature* 458 (7238), 619-622. <https://doi.org/10.1038/nature07857>.
- Hofmann, A. W., Jochum, K. P., Seufert, M., White, W. M., 1986. Nb and Pb in oceanic basalts: new constraints on mantle evolution. *Earth Planet. Sci. Lett.* 79, 33-45. [https://doi.org/10.1016/0012-821X\(86\)90038-5](https://doi.org/10.1016/0012-821X(86)90038-5).
- Jiang, Y. H., Jiang, S. Y., Ling, H. F., Ni, P., 2010. Petrogenesis and tectonic implications of Late Jurassic shoshonitic lamprophyre dikes from the Liaodong Peninsula, NE China. *Mineral. Petrol.* 100 (3-4), 127-151. <https://doi.org/10.1007/s00710-010-0124-8>.
- Kamenetsky, V. S., Crawford, A. J., Meffre, S., 2001. Factors Controlling Chemistry of Magmatic Spinel: an Empirical Study of Associated Olivine, Cr-spinel and Melt Inclusions from Primitive Rocks. *J. Petrol.* 42 (4), 655-671. <https://doi.org/10.1093/petrology/42.4.655>.
- Karato, S. I., 2011. Water distribution across the mantle transition zone and its implications for global material circulation. *Earth Planet. Sci. Lett.* 301 (3), 413-423. <https://doi.org/10.1016/j.epsl.2010.11.038>.
- Katz, R. F., Spiegelman, M., Langmuir, C. H., 2003. A new parameterization of hydrous mantle melting: *Geochem. Geophys. Geosyst.* 4 (9), 1073. <https://doi.org/10.1029/2002GC000433>.
- Kelley, K. A., Cottrell, E., 2009. Water and the Oxidation State of Subduction Zone Magmas. *Science*. 325(5940), 605-607. DOI:10.1126/science.1174156.
- Kuritani, T., Kimura, J.-I., Miyamoto, T., Wei, H., Shimano, T., Maeno, F., Jin, X., Taniguchi, H., 2009. Intraplate magmatism related to deceleration of upwelling

- asthenospheric mantle: Implications from the Changbaishan shield basalts, northeast China. *Lithos* 112, 247-258. <https://doi.org/10.1016/j.lithos.2009.02.007>.
- Kuritani, T., Ohtani, E., Kimura, J. I., 2011. Intensive hydration of the mantle transition zone beneath China caused by ancient slab stagnation. *Nat. Geosci.* 4 (10), 713-716. <https://doi.org/10.1038/ngeo1250>.
- Kuritani, T., Xia, Q. K., Kimura, J. I., Liu, J., Shimizu, K., Ushikubo, T., Zhao, D., Nakagawa, M., Yoshimura, S., 2019. Buoyant hydrous mantle plume from the mantle transition zone. *Sci. Rep.* 9 (1), 6549. <https://doi.org/10.1038/s41598-019-43103-y>.
- Kusky, T. M., 2011. Geophysical and geological tests of tectonic models of the North China Craton. *Gondwana Res.* 20 (1), 26-35. <https://doi.org/10.1016/j.gr.2011.01.004>.
- Lee, C.-T. A., Luffi, P., Plank, T., Dalton, H., Leeman, W. P., 2009. Constraints on the depths and temperatures of basaltic magma generation on Earth and other terrestrial planets using new thermobarometers for mafic magmas. *Earth Planet. Sci. Lett.* 279 (1), 20-33. <https://doi.org/10.1016/j.epsl.2008.12.020>.
- Li, S., Suo, Y., Li, X., Zhou, J., Santosh, M., Wang, P., Wang, G., Guo, L., Yu, S., Lan, H., Dai, L., Zhou, Z., Cao, X., Zhu, J., Liu, B., Jiang, S., Wang, G., Zhang, G., 2019. Mesozoic tectono-magmatic response in the East Asian ocean-continent connection zone to subduction of the Paleo-Pacific Plate. *Earth-Sci. Rev.* 192, 91-137. <https://doi.org/10.1016/j.earscirev.2019.03.003>.
- Liang, C., Liu, Y., Neubauer, F., Jin, W., Zeng, Z., Genser, J., Li, W., Li, W., Han, G., Wen, Q., Zhao, Y., Cai, L., 2015. Structural characteristics and LA-ICP-MS U-Pb zircon geochronology of the deformed granitic rocks from the Mesozoic Xingcheng-Taili ductile shear zone in the North China Craton. *Tectonophysics* 650, 80-103. <https://doi.org/10.1016/j.tecto.2014.05.010>.
- Liu, D. Y., Nutman, A. P., Compston, W., Wu, J. S., Shen, Q. H., 1992. Remnants of  $\geq 3800$  Ma crust in the Chinese part of the Sino-Korean craton. *Geology* 20. [https://doi.org/10.1130/0091-7613\(1992\)020<0339:ROMCIT>2.3.CO;2](https://doi.org/10.1130/0091-7613(1992)020<0339:ROMCIT>2.3.CO;2).
- Liu, J., Xia, Q.-K., Kuritani, T., Hanski, E., Yu, H.-R., 2017. Mantle hydration and the role of water in the generation of large igneous provinces. *Nat. Commun.* 8 (1), 1824. <https://doi.org/10.1038/s41467-017-01940-3>.
- Liu, Y., Wei, J., Zhang, D., Chen, J., Zhang, X., 2020. Early Cretaceous Wulong intermediate-mafic dike swarms in the Liaodong Peninsula: Implications for rapid lithospheric delamination of the North China Craton. *Lithos* 362-363, 105473. <https://doi.org/10.1016/j.lithos.2020.105473>.

- Ma, L., Jiang, S. Y., Hofmann, A. W., Dai, B. Z., Hou, M. L., Zhao, K. D., Chen, L. H., Li, J. W., Jiang, Y. H., 2014. Lithospheric and asthenospheric sources of lamprophyres in the Jiaodong Peninsula: A consequence of rapid lithospheric thinning beneath the North China Craton? *Geochim. Cosmochim. Acta* 124, 250-271. <https://doi.org/10.1016/j.gca.2013.09.035>.
- Ma, Q., Xu, Y. G., 2021. Magmatic perspective on subduction of Paleo-Pacific plate and initiation of big mantle wedge in East Asia. *Earth-Sci. Rev.* 213, 103473. <https://doi.org/10.1016/j.earscirev.2020.103473>.
- Matveenkov, VV; Sorokhtin, OG, 1998. Petrological peculiarities of the initial stages of development of intraplate volcanism of the Loihi Island (Hawaiian Archipelago). *Oceanology* 38 (5), 671-678.
- Mckenzie, D., Bickle, M. J., 1988. The Volume and Composition of Melt Generated by Extension of the Lithosphere. *J. Petrol.* 29 (3), 625-679. <https://doi.org/10.1093/petrology/29.3.625>.
- Murphy, D. T., Collerson, K. D., Kamber, B. S., 2002. Lamproites from Gaussberg, Antarctica: Possible Transition Zone Melts of Archaean Subducted Sediments. *J. Petrol.* 43 (6), 981-1001. <https://doi.org/10.1093/petrology/43.6.981>.
- Niu, Y., 2021. Lithosphere thickness controls the extent of mantle melting, depth of melt extraction and basalt compositions in all tectonic settings on Earth – A review and new perspectives. *Earth-Sci. Rev.* 217, 103614. <https://doi.org/10.1016/j.earscirev.2021.103614>.
- Norman, M. D., Garcia, M. O., 1999. Primitive magmas and source characteristics of the Hawaiian plume: petrology and geochemistry of shield picrites. *Earth Planet. Sci. Lett.* 168 (1), 27-44. [https://doi.org/10.1016/S0012-821X\(99\)00043-6](https://doi.org/10.1016/S0012-821X(99)00043-6).
- Pearce, J. A., 2008. Geochemical fingerprinting of oceanic basalts with applications to ophiolite classification and the search for Archean oceanic crust. *Lithos* 100 (1-4), 14-48. <https://doi.org/10.1016/j.lithos.2007.06.016>.
- Peng, L., Guo, J., 2019. Generation of Archaean TTG Gneisses Through Amphibole-dominated Fractionation. *J. Geophys. Res.: Solid Earth* 124 (4), 3605-3619. <https://doi.org/10.1029/2018JB017024>.
- Perinelli, C., Mollo, S., Gaeta, M., De Cristofaro, S. P., Palladino, D. M., Armienti, P., Scarlato, P., Putirka, K. D., 2016. An improved clinopyroxene-based hygrometer for Etnean magmas and implications for eruption triggering mechanisms. *Am. Mineral.* 101 (12), 2774-2777. <https://doi.org/10.2138/am-2016-5916>.
- Ray, R., Sheth, H. C., Mallik, J., 2007. Structure and emplacement of the Nandurbar–Dhule mafic dyke swarm, Deccan Traps, and the tectonomagmatic evolution of

- flood basalts. *Bull. of Volcanol.* 69 (5), 537-551. <https://doi.org/10.1007/s00445-006-0089-y>.
- Read, G., Grutter, H., Winter, S., Luckman, N., Gaunt, F., Thomsen, F., 2004. Stratigraphic relations, kimberlite emplacement and lithospheric thermal evolution, Quiricó Basin, Minas Gerais State, Brazil. *Lithos* 77, 803-818. <https://doi.org/10.1016/j.lithos.2004.04.011>.
- Reichow, M.K., Pringle, M.S., Al'Mukhamedov, A.I., Allen, M.B., Andreichev, V.L., Buslov, M.M., Davies, C.E., Fedoseev, G.S., Fitton, J.G., Inger, S., Medvedev, A.Y., Mitchell, C., Puchkov, V.N., Safonova, I.Y., Scott, R.A., Saunders, A.D., 2009. The timing and extent of the eruption of the Siberian Traps large igneous province: Implications for the end-Permian environmental crisis. *Earth Planet. Sci. Lett.* 277, 9-20. <https://doi.org/10.1016/j.epsl.2008.09.030>.
- Ren, Z.Y., Hanyu, T., Miyazaki, T., Chang, Q., Kawabata, H., Takahashi, T., Hirahara, Y., Nichols, A. R. L., Tatsumi, Y., 2009. Geochemical Differences of the Hawaiian Shield Lavas: Implications for Melting Process in the Heterogeneous Hawaiian Plume. *J. Petrol.* 50 (8), 1553-1573. <https://doi.org/10.1093/petrology/egp041>.
- Richard, G. C., Iwamori, H., 2010. Stagnant slab, wet plumes and Cenozoic volcanism in East Asia. *Phys. Earth and Planet. Inter.* 183 (1), 280-287. <https://doi.org/10.1016/j.pepi.2010.02.009>.
- Safonova, I., Maruyama, S., Litasov, K., 2015. Generation of hydrous-carbonate d plumes in the mantle transition zone linked to tectonic erosion and subduction. *Tectonophysics* 662, 454-471. <https://doi.org/10.1016/j.tecto.2015.08.005>.
- Saunders, A. D., Storey, M., Kent, R. W., Norry, M., 1992. Consequences of plume-lithosphere interactions. *Geol. Soc.* 68 (1), 41-60. <https://doi.org/10.1144/GSL.SP.1992.068.01.04>.
- Shimizu, K., Komiya, T., Hirose, K., Shimizu, N., Maruyama, S., 2001. Cr-spinel, an excellent micro-container for retaining primitive melts—implications for a hydrous plume origin for komatiites. *Earth Planet. Sci. Lett.* 189 (3), 177-188. [https://doi.org/10.1016/S0012-821X\(01\)00359-4](https://doi.org/10.1016/S0012-821X(01)00359-4).
- Smith, E. I., Sanchez, A., Walker, J. D., Wang, K., 1999. Geochemistry of mafic magmas in the Hurricane volcanic field, Utah: Implications for small- and large-scale chemical variability of the lithospheric mantle. *J. Geol.* 107 (4), 433-433. <https://doi.org/10.1086/314355>.
- Stern R. J., 2002. Subduction zones. *Rev. Geophys.* 40(4), 1012-1049. <https://doi.org/10.1029/2001RG000108>.

- Su, L., Song, S., Wang, C., Allen, M. B., Zhang, H., 2021. Picrite-basalt complex in the Baoshan-Gongshan Block of northern Sibumasu: Onset of a mantle plume before breakup of Gondwana and opening of the Neo-Tethys Ocean. *GSA Bulletin* 134 (5-6), 1091-1108. <https://doi.org/10.1130/B36028.1>.
- Sun, P., Niu, Y., Guo, P., Duan, M., Wang, X., Gong, H., Xiao, Y., 2020. The Lithospheric Thickness Control on the Compositional Variation of Continental Intraplate Basalts: A Demonstration Using the Cenozoic Basalts and Clinopyroxene Megacrysts From Eastern China. *J. Geophys. Res.: Solid Earth* 125 (3), e2019JB019315. <https://doi.org/10.1029/2019JB019315>.
- Sun, S. S., McDonough, W. F., 1989. Chemical and isotopic systematics of oceanic basalts: Implications for mantle composition and processes. *Geol. Soc., London, Special Publications* 42 (1), 313-345. <https://dx.doi.org/10.1144/GSL.SP.1989.042.01.19>.
- Sun, Y., Ying, J., Zhou, X., Shao, J. a., Chu, Z., Su, B., 2014. Geochemistry of ultrapotassic volcanic rocks in Xiaogulihe NE China: Implications for the role of ancient subducted sediments. *Lithos* 208-209, 53-66. <https://doi.org/10.1016/j.lithos.2014.08.026>.
- Tappe, S., Ngwenya, N.S., Stracke, A., Romer, R.L., Glodny, J., Schmitt, A.K., 2023. Plume–lithosphere interactions and LIP-triggered climate crises constrained by the origin of Karoo lamproites. *Geochim. Cosmochim. Acta* 350, 87-105. <https://doi.org/10.1016/j.gca.2023.04.008>.
- Tappe, S., Romer, R.L., Stracke, A., Steinfeld, A., Smart, K.A., Muehlenbachs, K., Torsvik, T.H., 2017. Sources and mobility of carbonate melts beneath cratons, with implications for deep carbon cycling, metasomatism and rift initiation. *Earth Planet. Sci. Lett.* 466, 152-167. <https://doi.org/10.1016/j.epsl.2017.03.011>.
- Tappe, S., Smart, K.A., Stracke, A., Romer, R.L., Prelević, D., van den Bogaard, P., 2016. Melt evolution beneath a rifted craton edge:  $^{40}\text{Ar}/^{39}\text{Ar}$  geochronology and Sr–Nd–Hf–Pb isotope systematics of primitive alkaline basalts and lamprophyres from the SW Baltic Shield. *Geochim. Cosmochim. Acta* 173, 1-36. <https://doi.org/10.1016/j.gca.2015.10.006>.
- Tappe, S., Foley, S.F., Stracke, A., Romer, R.L., Kjarsgaard, B.A., Heaman, L.M., Joyce, N., 2007. Craton reactivation on the Labrador Sea margins:  $^{40}\text{Ar}/^{39}\text{Ar}$  age and Sr–Nd–Hf–Pb isotope constraints from alkaline and carbonatite intrusives. *Earth Planet. Sci. Lett.* 256, 433-454. <https://doi.org/10.1016/j.epsl.2007.01.036>.
- Tatsumoto, M., Basu, A. R., Wankang, H., Junwen, W., Guanghong, X., 1992. Sr, Nd, and Pb isotopes of ultramafic xenoliths in volcanic rocks of Eastern China:

- enriched components EMI and EMII in subcontinental lithosphere. *Earth Planet. Sci. Lett.* 113 (1-2), 107-128. [https://doi.org/10.1016/0012-821X\(92\)90214-G](https://doi.org/10.1016/0012-821X(92)90214-G).
- Tenner, T. J., Hirschmann, M. M., Withers, A. C., Ardia, P., 2012. H<sub>2</sub>O storage capacity of olivine and low-Ca pyroxene from 10 to 13 GPa: consequences for dehydration melting above the transition zone. *Contrib. Mineral. Petrol.* 163 (2), 297-316. <https://doi.org/10.1007/s00410-011-0675-7>.
- Wan, L., Zeng, Z., Kusky, T., Asimow, P., He, C., Liu, Y., Yang, S., Xu, S., 2019. Geochemistry of middle-late Mesozoic mafic intrusions in the eastern North China Craton: New insights on lithospheric thinning and decratonization. *Gondwana Res.* 73, 153-174. <https://doi.org/10.1016/j.gr.2019.04.004>.
- Wang, C., Song, S., Niu, Y., Wei, C., Su, L., 2016. TTG and Potassic Granitoids in the Eastern North China Craton: Making Neoproterozoic Upper Continental Crust during Micro-continental Collision and Post-collisional Extension. *J. Petrol.* 57 (9), 1775-1810. <https://doi.org/10.1093/petrology/egw060>.
- Wang, C., Song, S., Su, L., Allen, M. B., 2022. Crustal maturation and cratonization in response to Neoproterozoic continental collision: The Suizhong granitic belt, North China Craton. *Precambrian Res.* 377, 106732. <https://doi.org/10.1016/j.precamres.2022.106732>.
- Wang, C., Song, S., Su, L., Allen, M. B., Dong, J., 2021. Lithospheric modification at the onset of the destruction of the North China Craton: Evidence from Late Triassic mafic dykes. *Chem. Geol.* 566 (1), 120105. <https://doi.org/10.1016/j.chemgeo.2021.120105>.
- Wang, C., Song, S., Wei, C., Su, L., Dong, J., 2019. Palaeoproterozoic deep mantle heterogeneity recorded by enriched plume remnants. *Nat. Geosci.* 12 (8), 672-678. <https://doi.org/10.1038/s41561-019-0410-y>.
- Wang, X. C., Wilde, S. A., Li, Q.-L., Yang, Y.-N., 2015. Continental flood basalts derived from the hydrous mantle transition zone. *Nat. Commun.* 6 (1), 7700. <https://doi.org/10.1038/ncomms8700>.
- Wu, F. Y., Lin, J. Q., Wilde, S. A., Zhang, X. O., Yang, J. H., 2005. Nature and significance of the Early Cretaceous giant igneous event in eastern China. *Earth Planet. Sci. Lett.* 233 (1-2), 103-119. <https://doi.org/10.1016/j.epsl.2005.02.019>.
- Wu, F. Y., Walker, R. J., Yang, Y. H., Yuan, H. L., Yang, J. H., 2006a. The chemical-temporal evolution of lithospheric mantle underlying the North China Craton. *Geochim. Cosmochim. Acta* 70 (19), 5013-5034. <https://doi.org/10.1016/j.gca.2006.07.014>.
- Wu, F. Y., Yang, J. H., Zhang, Y. B., 2006b. Emplacement ages of the Mesozoic granites in southeastern part of the Western Liaoning Province. *Acta Petrol. Sin.*

22 (2), 315-325. doi: 1000-0569/2006/022(02)-0315-25 (in Chinese with English abstract).

- Wu, F. Y., Yang, J. H., Xu, Y. G., Wilde, S. A., Walker, R. J., 2019. Destruction of the North China Craton in the Mesozoic. *Annu. Rev. Earth Planet. Sci.* 47, 1. <https://doi.org/10.1146/annurev-earth-053018-060342>.
- Wu, Z., Wang, C., Song, S., Allen, M. B., Kusky, T., Su, L., 2022. Ultrahigh-pressure peridotites record Neoproterozoic collisional tectonics. *Earth Planet. Sci. Lett.* 596, 117787. <https://doi.org/10.1016/j.epsl.2022.117787>.
- Xia, Q., Liu, J., Zhang, B., Li, P., Gu, X., Chen, H., 2022. Water and partial melting in the Earth's mantle. *Acta Petrol. Sin.* 38(12), 3631-3646. DOI: 10.18654/1000-0569/2022. 12.04 (in Chinese with English abstract).
- Xu, W., Zhu, D. C., Wang, Q., Weinberg, R. F., Wang, R., Li, S. M., Zhang, L. L., Zhao, Z. D., 2019. Constructing the Early Mesozoic Gangdese Crust in Southern Tibet by Hornblende-dominated Magmatic Differentiation. *J. Petrol.* 60, 515-552. <https://doi.org/10.1093/petrology/egz005>.
- Xu, Y., Li, H., Pang, C., He, B., 2009. On the timing and duration of the destruction of the North China Craton. *Chin. Sci. Bull.* 54, 1974-1989. <https://doi.org/10.1007/s11434-009-0346-5>.
- Xu, Y. G., 2001. Thermo-tectonic destruction of the archaean lithospheric keel beneath the Sino-Korean Craton in China: Evidence, timing and mechanism: *Phys. Chem. Earth, Part A. Solid Earth and Geodesy* 26, 747-757. [https://doi.org/10.1016/S1464-1895\(01\)00124-7](https://doi.org/10.1016/S1464-1895(01)00124-7).
- Yang, J. H., Chung, S. L., Wilde, S. A., Wu, F. Y., Chu, M. F., Lo, C. H., Fan, H. R., 2005. Petrogenesis of post-orogenic syenites in the Sulu Orogenic Belt, East China: geochronological, geochemical and Nd-Sr isotopic evidence. *Chem. Geol.* 214 (1-2), 99-125. <https://doi.org/10.1016/j.chemgeo.2004.08.053>.
- Yang, J. H., Wu, F. Y., Simon A. Wildesupp, Fukun Chensup, Liu, X. M., Xie, L. W., 2008a. Petrogenesis of an Alkali Syenite-Granite-Rhyolite Suite in the Yanshan Fold and Thrust Belt, Eastern North China Craton: Geochronological, Geochemical and Nd-Sr-Hf Isotopic Evidence for Lithospheric Thinning. *J. Petrol.* 49 (2), 315-35. <https://doi.org/10.1093/petrology/egm083>.
- Yang, J. H., Sun, J. F., Chen, F., Wilde, S. A., Wu, F. Y., 2008b. Sources and Petrogenesis of Late Triassic Dolerite Dikes in the Liaodong Peninsula: Implications for Post-collisional Lithosphere Thinning of the Eastern North China Craton. *J. Petrol.* 48 (10), 1973-1997. <https://doi.org/10.1093/petrology/egm046>.
- Zhai, M., Zhao, L., Zhu, X., Zhou, Y., Peng, P., Guo, J., Li, Q., Zhao, T., Lu, J., Li, X.,

2021. Late Neoproterozoic magmatic–metamorphic event and crustal stabilization in the North China Craton. *Am. J. Sci.* 321 (1-2), 206-234. <https://doi.org/10.2475/01.2021.06>.
- Zhang, S. H., Zhao, Y., Davis, G. A., Ye, H., Wu, F., 2014. Temporal and spatial variations of Mesozoic magmatism and deformation in the North China Craton: Implications for lithospheric thinning and decratonization. *Earth-Sci. Rev.* 131, 49-87. <https://doi.org/10.1016/j.earscirev.2013.12.004>.
- Zhao, J. H., Zhou, M. F., 2007. Geochemistry of Neoproterozoic mafic intrusions in the Panzihua district (Sichuan Province, SW China): Implications for subduction-related metasomatism in the upper mantle. *Precambrian Res.* 152, 27-47. <https://doi.org/10.1016/j.precamres.2006.09.002>.
- Zhao, D., Tian, Y., 2013. Changbai intraplate volcanism and deep earthquakes in East Asia: a possible link? *Geophys. J. Int.* 195 (2), 706-724. <https://doi.org/10.1093/gji/ggt289>.
- Zhao, G., Sun, M., Wilde, S. A., Sanzhong, L., 2005. Late Archean to Paleoproterozoic evolution of the North China Craton: key issues revisited. *Precambrian Res.* 136 (2), 177-202. <https://doi.org/10.1016/j.precamres.2004.10.002>.
- Zhao, G., Wilde, S. A., Cawood, P. A., Sun, M., 2001. Archean blocks and their boundaries in the North China Craton: lithological, geochemical, structural and P–T path constraints and tectonic evolution. *Precambrian Res.* 107 (1-2), 0-73. [https://doi.org/10.1016/S0301-9268\(00\)00154-6](https://doi.org/10.1016/S0301-9268(00)00154-6).
- Zheng, J., Sun, M., Zhou, M.-F., Robinson, P., 2005. Trace elemental and PGE geochemical constraints of Mesozoic and Cenozoic peridotitic xenoliths on lithospheric evolution of the North China Craton. *Geochim. Cosmochim. Acta* 69 (13), 3401-3418. <https://doi.org/10.1016/j.gca.2005.03.020>.
- Zheng, Y., Chen, R., Zheng, X., Zhang, S., 2016. The transport of water in subduction zones. *Sci. China: Earth Sci.* 59 (4), 651-682. <https://doi.org/10.1007/s11430-015-5258-4>.
- Zheng, Y., Xu, Z., Zhao, Z., Dai, L., 2018. Mesozoic mafic magmatism in North China: Implications for thinning and destruction of cratonic lithosphere. *Sci. China: Earth Sci.* 61 (4), 353-385. <https://doi.org/10.1007/s11430-017-9160-3>.
- Zhu, G., Gerya, T. V., Yuen, D. A., Honda, S., Yoshida, T., Connolly, J. A. D., 2009. Three-dimensional dynamics of hydrous thermal-chemical plumes in oceanic subduction zones. *Geochem. Geophys. Geosyst.* 10 (11). <https://doi.org/10.1029/2009GC002625>.
- Zhu, R. X., Xu, Y. G., 2019. The subduction of the west Pacific plate and the destruction of the North China Craton. *Sci. China: Earth Sci.* 62 (9), 1340-1350.

<https://doi.org/10.1007/s11430-018-9356-y>.

Zhu, R. X., Yang, J. H., Wu, F. Y., 2012. Timing of destruction of the North China Craton. *Lithos* 149, 51-60. <https://doi.org/10.1016/j.lithos.2012.05.013>.

### Figure captions

**Figure 1.** (a) Histogram of ages from Jurassic to Cretaceous igneous rocks and dykes in the Taihang to Western Liaoning region of the Eastern NCC. (b) Topographic map showing the NCC and adjacent regions based on the ETOPO1 Global Relief Model (<https://www.ngdc.noaa.gov/mgg/global/>). (c) Simplified geological map of the Eastern NCC, with the study regions (Figs. 1d, e) indicated by rectangles (modified after Geological map of NCC, 1:250,000). (d, e) Geological maps of the Xingcheng and Taili region in Western Liaoning, respectively. Insets d1, e1: Rose diagrams showing the strikes of the mafic dyke swarms. Age data are from references in Supplemental Table S1.

**Figure 2.** Field and microphotographs of mafic dykes in Western Liaoning, NCC. (a) The picritic dyke swarm (more than 3 parallel dykes out of the view) in the Taili region. (b) The picritic dyke swarm in the Xingcheng region. (c) The potassic mafic dyke swarm intruded into the Mesoproterozoic strata, and (d), into the Archean potassic granite in the Xingcheng region. (e) Olivine pseudocrystals altered by iddingsite in the fine-grained matrix. (f) Porphyritic texture with Cpx xenocrysts and fine-grained groundmass. (g) Euhedral to subhedral spinel grains in the picritic dyke sample (backscattered electron image). (h) The ophitic texture of potassic mafic dykes with Cpx xenocryst with amphibole and plagioclase. Cpx, clinopyroxene; Hb, hornblende; Pl, plagioclase; Sp, spinel.

**Figure 3.** Zircon U-Pb concordia diagrams of zircon U-Pb isotope analysis and representative cathodoluminescence images of zircons for mafic dykes from the Taili and Xingcheng regions.

**Figure 4.** (a) Wo-En-Fs diagram for clinopyroxene. (b)  $X_{Mg}$ -Si diagram for magmatic hornblende. (c) Chromian spinel compositions in the picritic mafic dykes. Also shown are MORB, LIP, OIB, and SSZ fields after (Kamenetsky et al., 2001). MORB: mid-ocean ridge basalts; LIP: large igneous province; OIB: ocean island basalts; SSZ: Supra-subduction zone.

**Figure 5.** Classification diagrams of mafic dyke swarms in Western Liaoning. (a) TAS

diagram of total alkalis vs.  $\text{SiO}_2$ . (b) Plot of  $\text{SiO}_2$  versus  $\text{MgO}$ . (c)  $\text{Zr/TiO}_2$  vs.  $\text{Nb/Y}$  diagram. (d) Plot of  $\text{K}_2\text{O}$  vs.  $\text{SiO}_2$ . The data for the Taili lamprophyres are from Wan et al. (2019). The data for the Huaziyu lamprophyres are from Jiang et al. (2010). The data of Hawaiian picrites are from Hanyu et al., (2010), Matveenkov et al. (1998), Norman and Garcia (1999), and Ren et al. (2009). The data of Changbaishan basalts are from Kuritani et al. (2009).

**Figure 6.** Chondrite-normalized REE patterns and Primitive mantle-normalized trace element spidergrams for the Jurassic picritic dyke swarms (a,b) and potassic mafic dyke swarms (c, d) from the Western Liaoning, NCC. The values of chondrite and primitive mantle are from Sun and McDonough (1989). The data for ocean island basalt (OIB) and enriched mid-ocean-ridge basalt (E-MORB) are from Sun and McDonough (1989). Data sources are the same as in Figure 5.

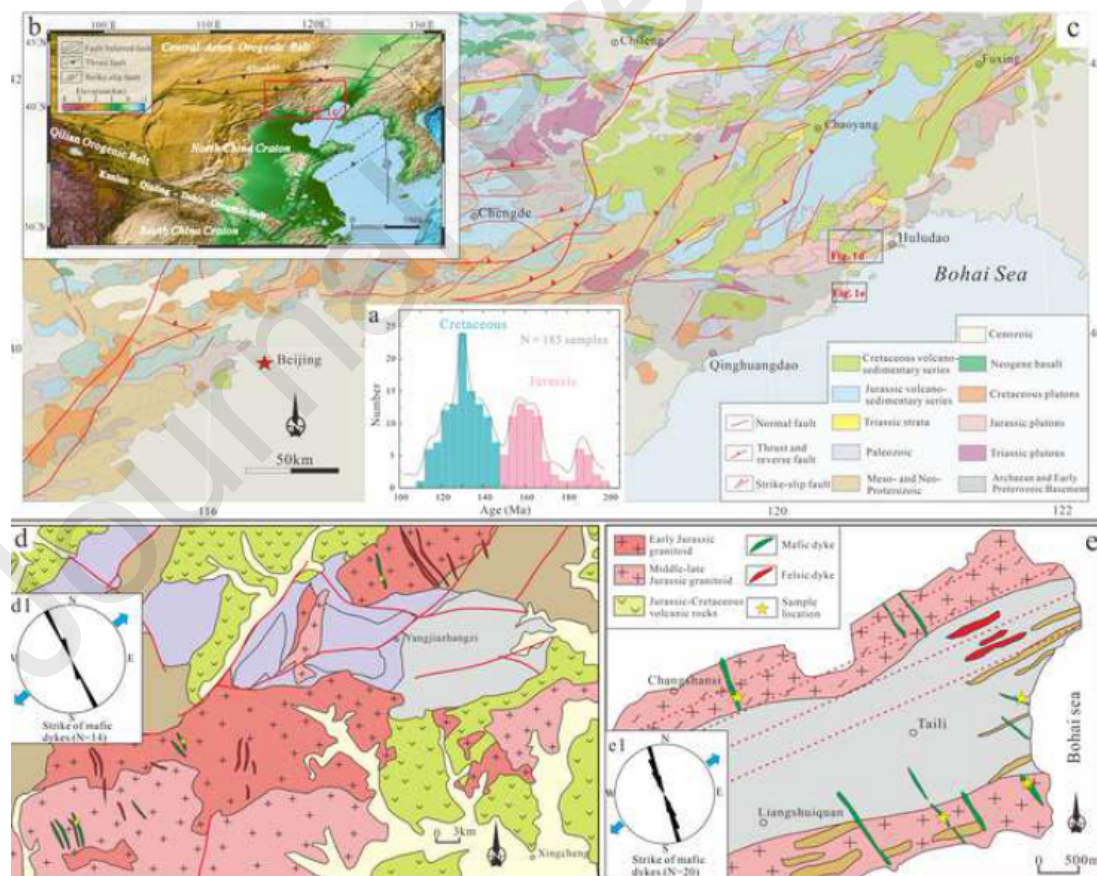
**Figure 7.**  $\epsilon\text{Nd}(t)$ -( $^{87}\text{Sr}/^{86}\text{Sr}$ )<sub>i</sub> diagram for the Jurassic picritic and potassic mafic dyke swarms from the Western Liaoning. Also compared are those of the ancient subcontinental lithospheric mantle (SCLM) of the North China Craton (Zhang and Yang, 2007), Cenozoic basalts from Tatsumoto et al. (1992). Data sources are the same as in Fig. 5.

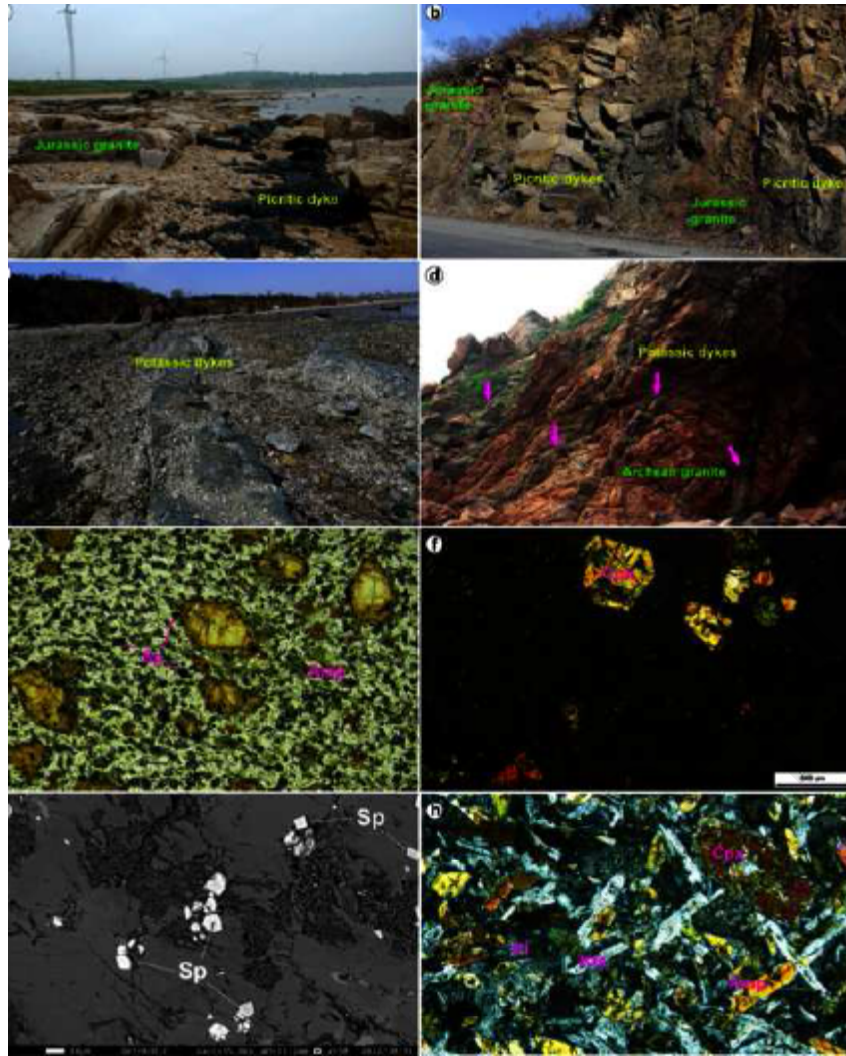
**Figure 8.** Plots of (a)  $\text{La/Ba}$  vs.  $\text{La/Nb}$  (Saunders et al., 1992), (b)  $\text{Nb/La}$  vs.  $\text{La/Yb}$  (Smith et al., 1999), (c)  $(\text{Hf/Sm})_N$  vs.  $(\text{Ta/La})_N$  (Flèche et al., 1998), (d)  $\text{Th/Yb}$  vs.  $\text{Nb/Yb}$  (Pearce, 2008) for the Jurassic picritic and potassic mafic dyke swarms from the Western Liaoning. SMLM = subduction-modified lithospheric mantle, SMAM = subduction-modified asthenospheric mantle, OIB = ocean island basalt, N-MORB = normal mid-ocean-ridge basalt, E-MORB = enriched mid-ocean-ridge basalt. The compositions of OIB, N-MORB, E-MORB are from Sun and McDonough (1989). Data sources are the same as in Fig. 5.

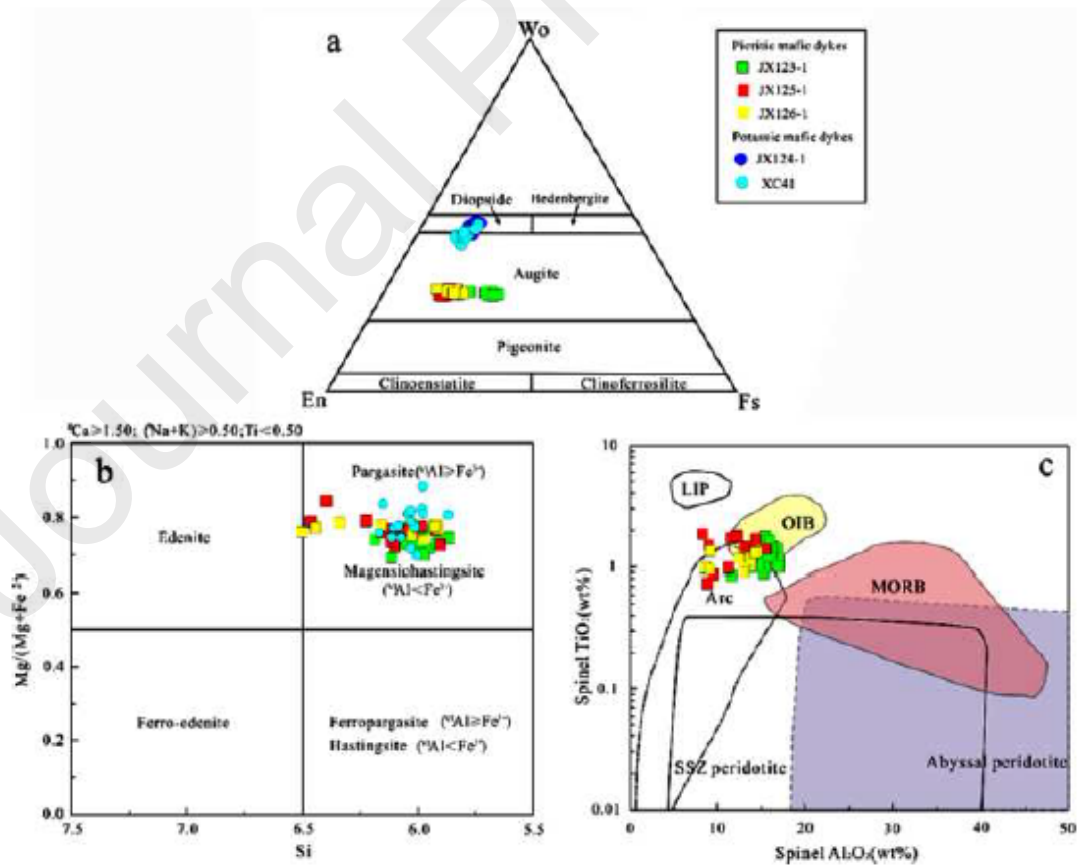
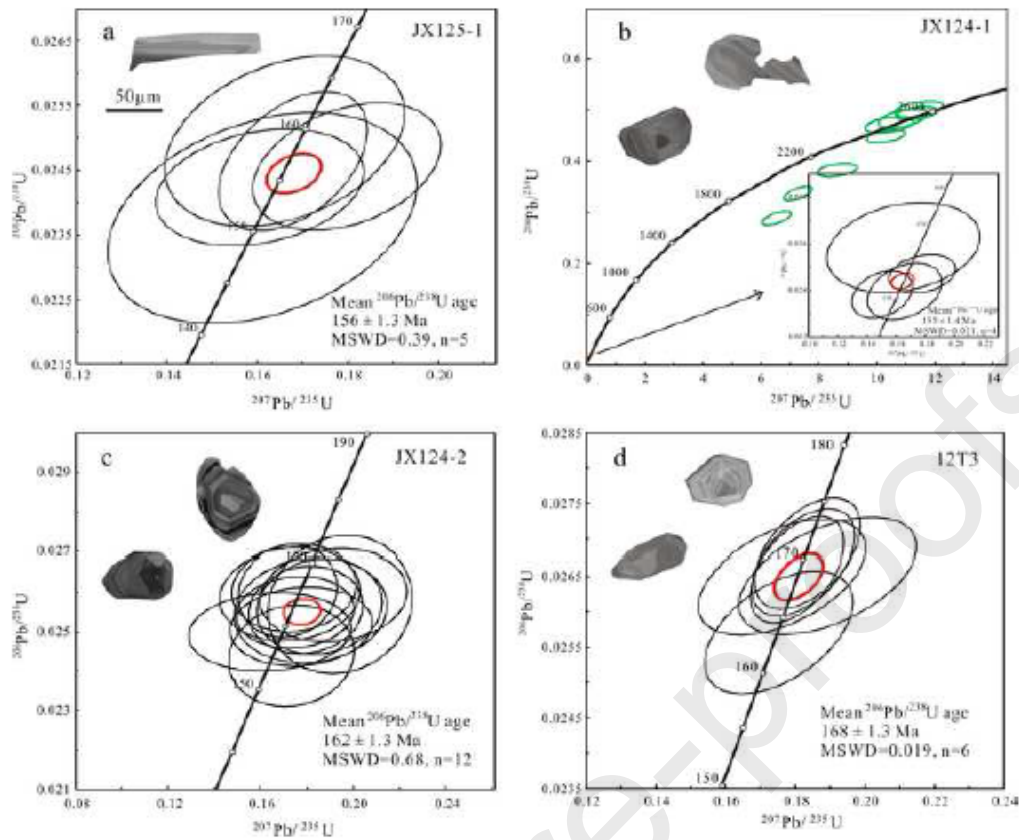
**Figure 9.** Pressure vs temperature conditions for the Jurassic picritic and potassic mafic dyke swarms in the Western Liaoning, NCC under different water contents. The dry lherzolite solidus and liquidus are from Katz et al. (2003). The melting conditions for mid-ocean ridge basalts (MORB), Paleoproterozoic komatiites are from Lee et al. (2009), and data sources of Hawaii hotspot picrites are the same as in Fig. 5.

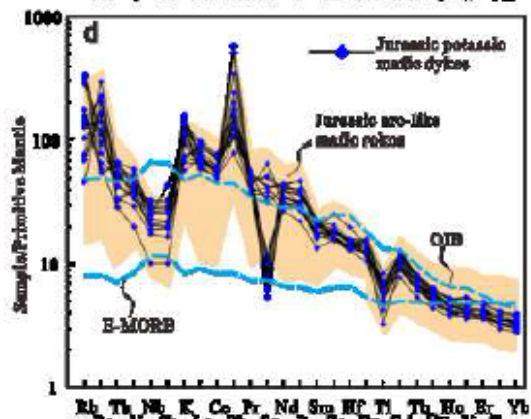
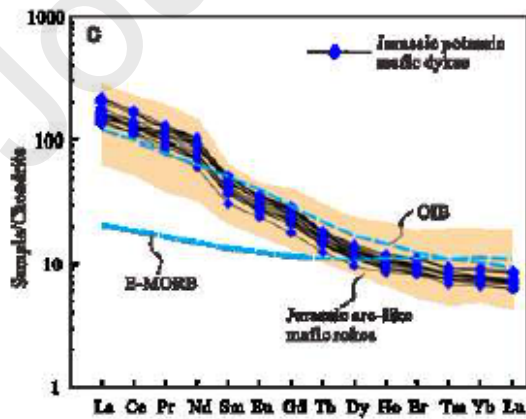
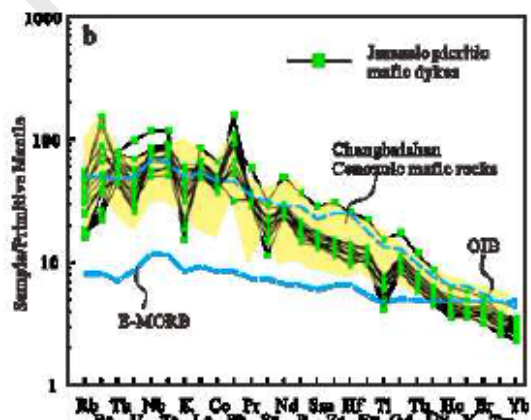
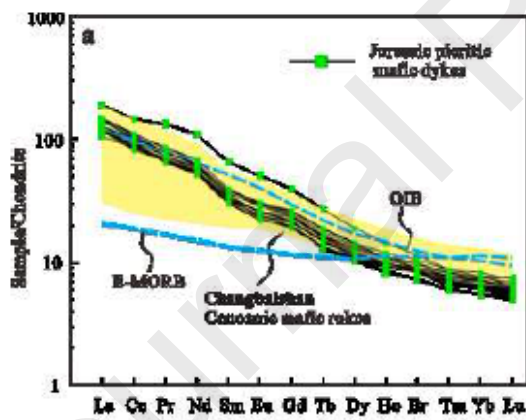
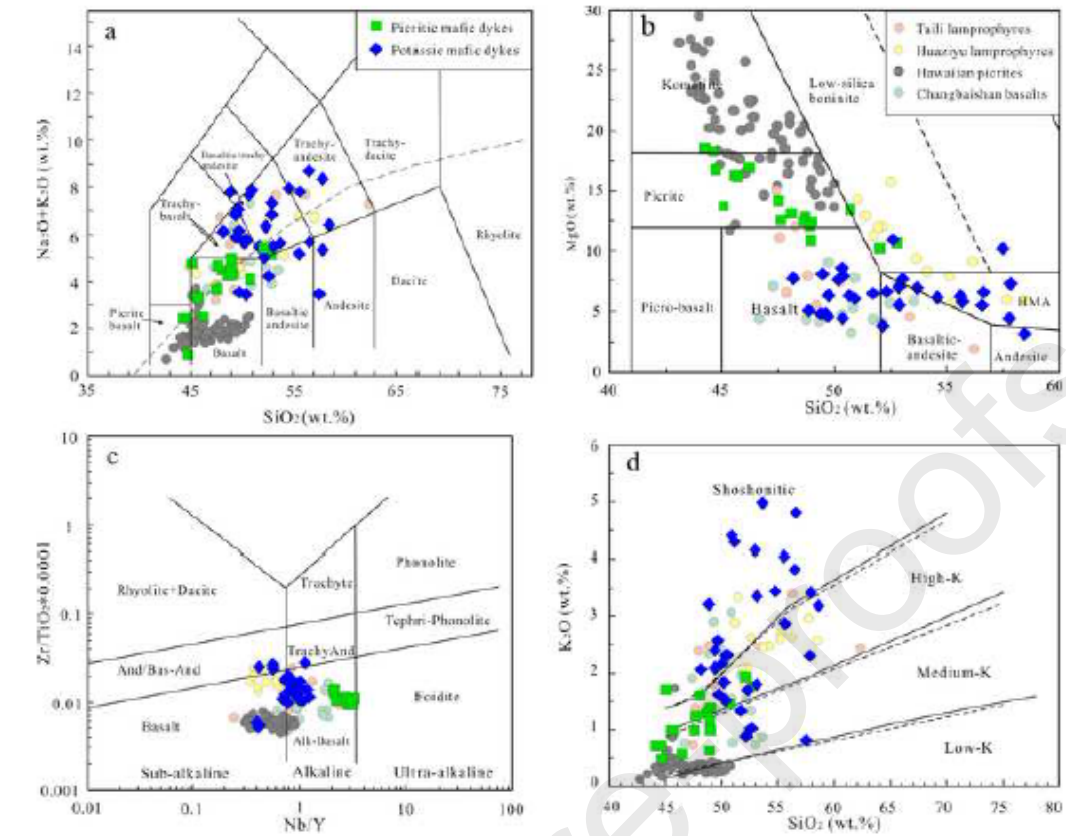
**Figure 10.**  $\text{Dy/Yb}$  vs.  $\text{K/Yb} \times 1000$  (Duggen et al., 2005) discrimination diagrams for the Jurassic picritic and potassic mafic dyke swarms from the Western Liaoning.

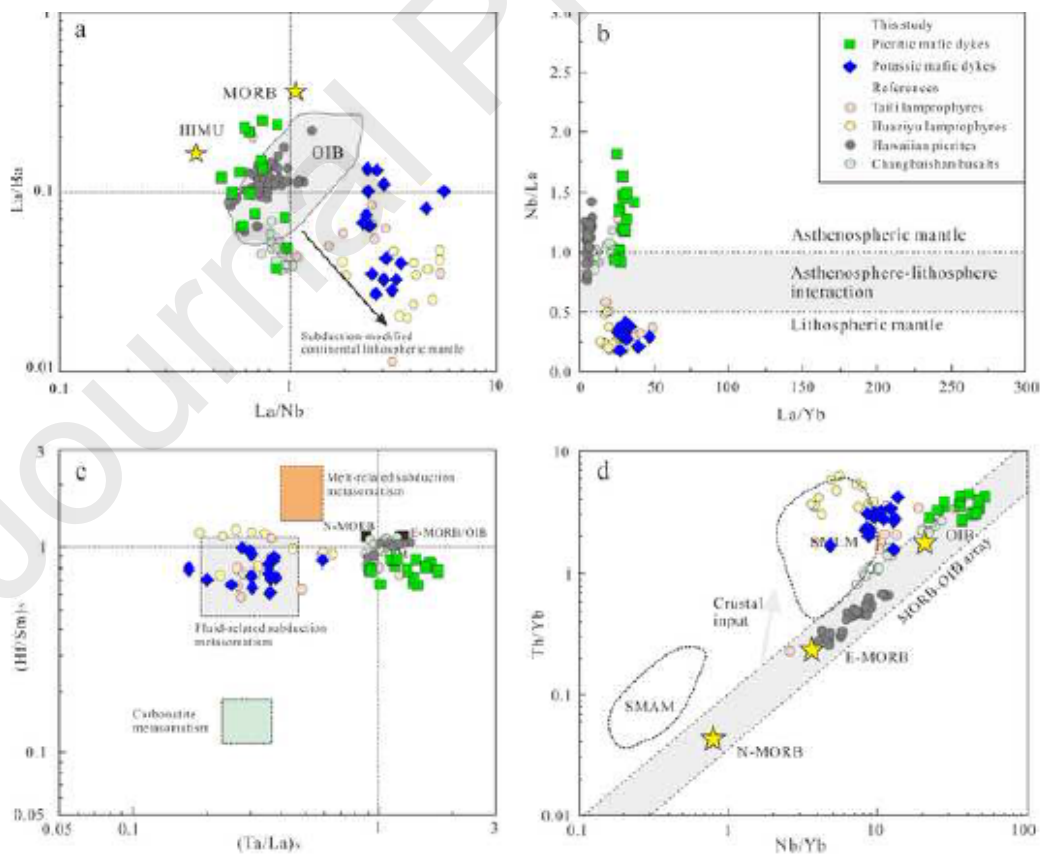
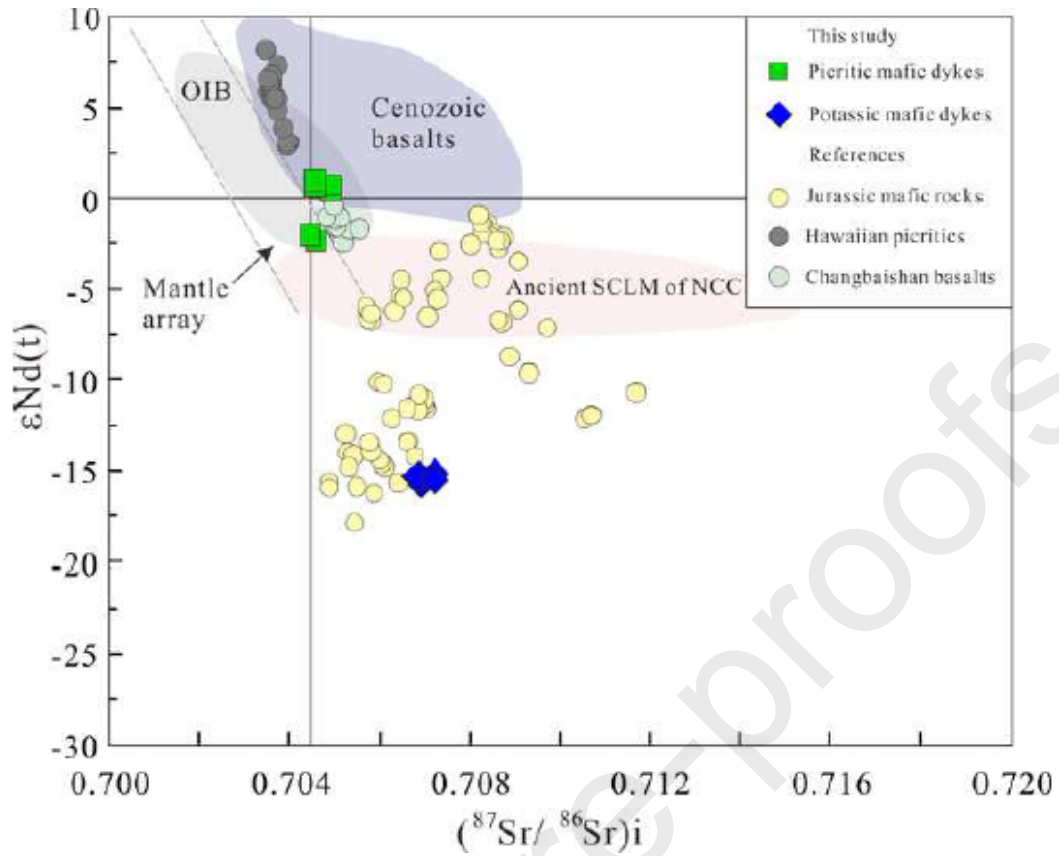
**Figure 11.** (a) The hydrous asthenospheric mantle melts formed beneath the NCC during the Jurassic Paleo-Pacific subduction. (b) Schematic diagram of the origin of the hydrous asthenospheric from the hydrous mantle transition zone during the Jurassic flat subduction of the Paleo-Pacific plate. The slab reached the mantle transformation zone (MTZ). Initially cold slab was subjected to conductive heat from the surrounding mantle, causing volatilization of the slab, while deep earthquakes can also cause dehydration of the Paleo-Pacific plate (Zhao and Tian, 2013). Moreover, the dehydration of the slab peridotite in the MTZ will cause the rehydration of peridotite (Safonova et al., 2015). When the hydrous asthenospheric mantle melts are formed, it will rise from the MTZ to the upper mantle, dehydration melting should occur due to the decrease in water solubility in the constituent nominally anhydrous minerals (Tenner et al., 2012). (c) Conceptual schematic cartoon illustrating the formation of picritic and potassic mafic dyke swarms in western Liaoning, NCC. (d) Schematic model of Jurassic picritic and potassic dyke emplacement. (e) Tectonic evolutionary model and tectonic stress state of middle and late Jurassic in East China (modified after Li et al., 2019).

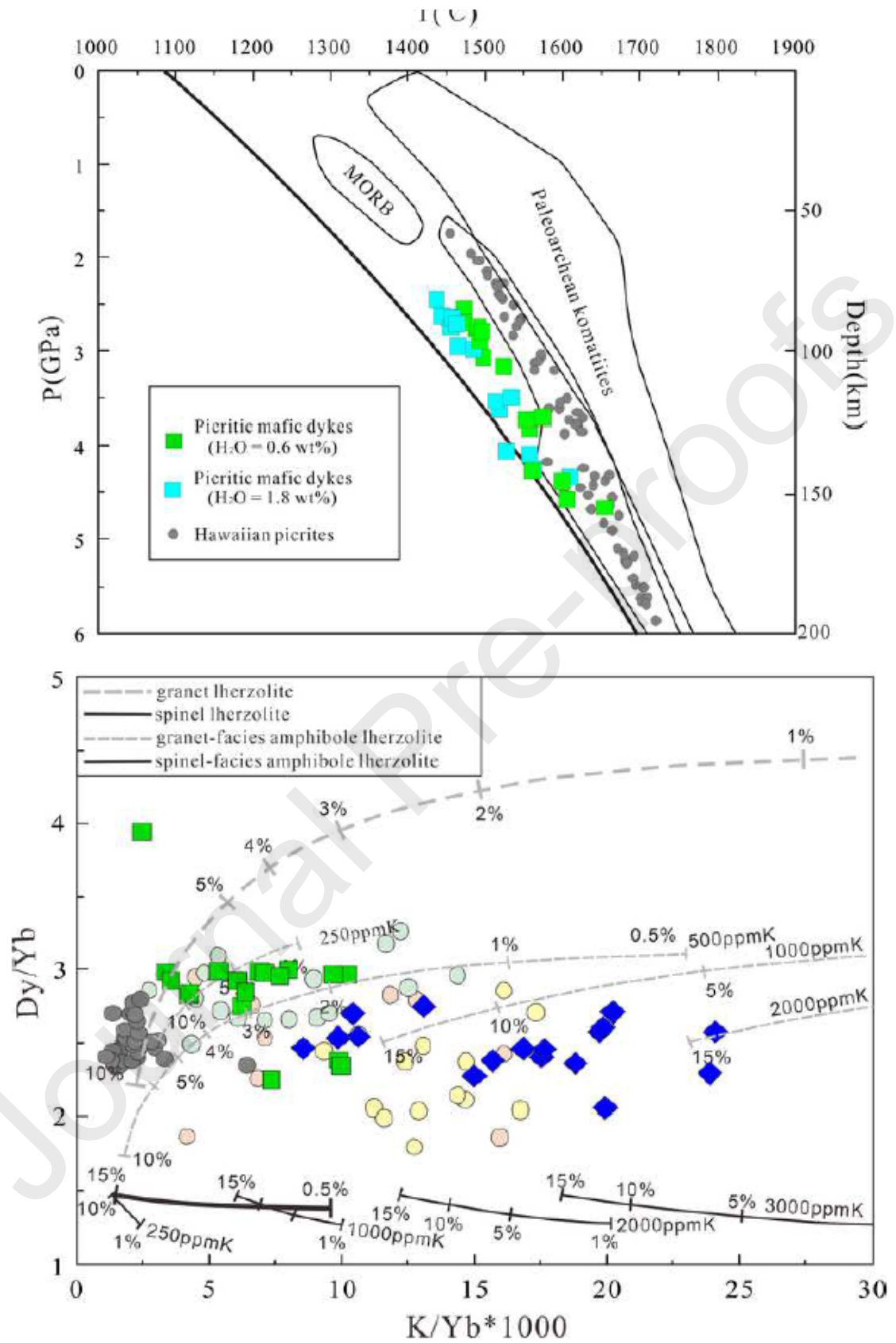


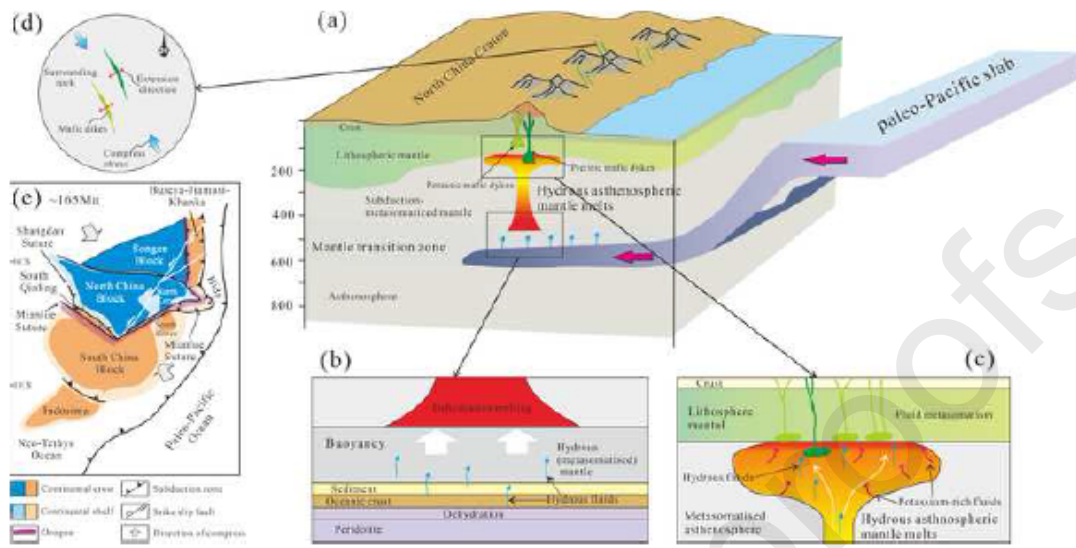














**Citation on deposit:**

Wang, W., Song, S., Wang, C., Allen, M. B., Zhang, L., Li, X., & Su, L. (2025). Jurassic picritic and potassic mafic dyke swarms in eastern China: Evidence for thermal erosion of the lithospheric mantle during Paleo-Pacific subduction. *Gondwana Research*, <https://doi.org/10.1016/j.gr.2025.02.012>

**For final citation and metadata, visit Durham Research Online URL:**

<https://durham-repository.worktribe.com/output/3550387>

**Copyright Statement:**

This accepted manuscript is licensed under the Creative Commons Attribution 4.0 licence. <https://creativecommons.org/licenses/by/4.0/>